



A Tutorial for Understanding Chemical Reactivity Through the Valence Bond Approach

Journal:	<i>Chemical Society Reviews</i>
Manuscript ID:	CS-REV-01-2014-000043.R1
Article Type:	Tutorial Review
Date Submitted by the Author:	25-Mar-2014
Complete List of Authors:	Shaik, Sason; Hebrew University Jerusalem, Chemistry Dandamudi, Usharani; Hebrew University, Institute of Chemistry Danovich, David; The Hebrew University, Institute of Chemistry, Institute of Chemistry Li, Chunsen; State Key Laboratory of Structural Chemistry, Fujian Institute of Research on the Structure of Matter, Chinese Academy of Sciences, Theoretical and Computational Department Lai, Wenzhen; Renmin University of China, Department of Chemistry Chen, Hui; Institute of Chemistry, Chinese Academy of Sciences, CAS Key Laboratory of Photochemistry

A Tutorial for Understanding Chemical Reactivity Through The Valence Bond Approach

Dandamudi Usharani,^a Wenzhen Lai,^b Chunsen Li,^c Hui Chen,^d David
Danovich^a and Sason Shaik,^{a*}

^a Institute of Chemistry and The Lise Meitner-Minerva Center for Computational Quantum Chemistry, The
Hebrew University of Jerusalem, 91904, Jerusalem, Israel

^b Department of Chemistry, Renmin University of China, Beijing, 100872, China

^c State Key Laboratory of Structural Chemistry, Fujian Institute of Research on the Structure of Matter,
Chinese Academy of Sciences, Fuzhou, Fujian 350002, China; Fujian Provincial Key Laboratory of
Theoretical and Computational Chemistry, Xiamen, Fujian 361005, China

^d Beijing National Laboratory for Molecular Sciences (BNLMS), CAS Key Laboratory of Photochemistry,
Institute of Chemistry, Chinese Academy of Sciences, Beijing, 100190, China

Email ID: sason@yfaat.ch.huji.ac.il

KEY LEARNING POINTS

- (1) VBSCD is a *valence bond state correlation diagram* wherein the correlation is dictated by the book keeping of electrons and bonds along the reaction coordinate.
- (2) VBSCD allows estimating barriers. The expression for reaction families: $\Delta E^\ddagger = fG_r - B$; ΔE^\ddagger is the barrier, G_r the promotion gap at the reactant side. ΔE^\ddagger is the balance between fG_r , the energy expense needed to achieve a transition state, and B the resonance energy of the transition state. Another equation that considers explicitly the promotion gaps for reactants and products, the corresponding f factors, and the thermodynamic driving force of the reaction, allows barrier estimation for large data sets. This is exemplified for 45 hydrogen-atom transfer (HAT) reactions, $X^\bullet + \text{H-Y} \rightarrow \text{X-H} + \text{Y}^\bullet$.
- (3) The VB approach elucidates mechanisms and enables to predict barriers from raw data such as bond dissociation energy (BDE), vertical bond energy (D) and radical reorganization energy (RE). Applications to HAT reactions demonstrate that the RE for the radicals (X^\bullet and Y^\bullet) is a key factor of the HAT barrier
- (4) The VB model makes bridges to rate-equilibrium relationships, and reveals new features, e.g. the promotion energy gap principle and entangled reactivity effects.
- (5) VBCMD is a *valence bond configuration-mixing diagram* that illustrates how intermediate-states and excited states govern mechanisms, selectivity and reactivity.

Abstract: This is a tutorial on the usage of valence bond (VB) diagrams for understanding chemical reactivity in general, and hydrogen atom transfer (HAT) reactivity in particular. The tutorial instructs the reader how to construct the VB diagrams and how to estimate HAT barriers from raw data, starting with the simplest reaction $\text{H} + \text{H}_2$ and going all the way to HAT in the enzyme Cytochrome P450. Other reactions are treated as well, and some unifying principles are outlined. The tutorial projects the unity of reactivity treatments, following Coulson's dictum "*give me insight, not numbers*", albeit with its modern twist: giving numbers and insight.

1. Introduction

1.1. General Introduction

Insight is essential. In the early days of quantum chemistry, since the 1930s onwards to the 1970s, the computational tools were meager and great quantum chemists were using their wits to generate useful concepts for chemistry by constructing simple and elegant models, such as Hund's Rule,¹ crystal field theory,² hybridization and resonance theory,³ frontier molecular orbital (FMO) theory,⁴ orbital symmetry rules,⁵ and so on.

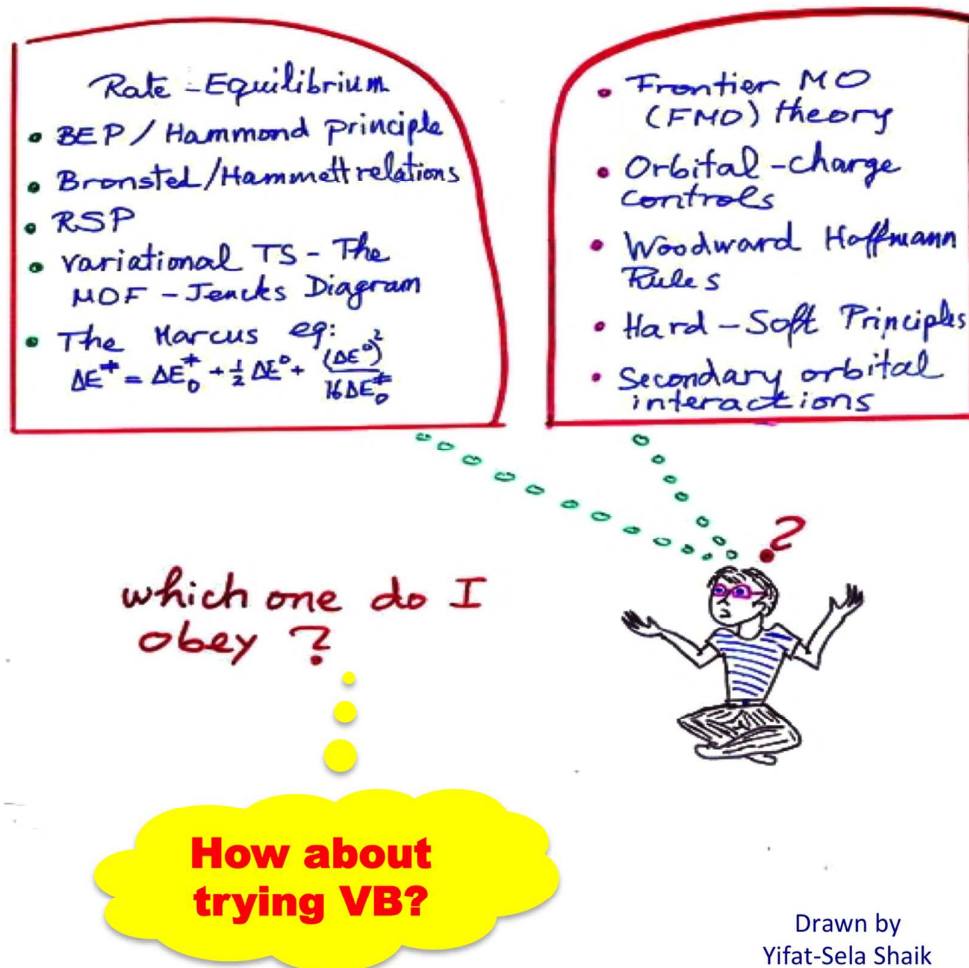
From the 1970s onwards, the computational tools began to improve in an accelerated pace, and getting the "right answer for the right reason" became the goal of most quantum chemists, who were using wave function theoretic (WFT) methods. The "number" has gradually gained increasing importance in the chemical community as theory was becoming a partner of experiment and serving as a spectrometer for generating observables.⁶

When density functional theory (DFT) entered chemistry it became possible to compute increasingly larger molecules, and obtain often surprisingly good "numbers". The use of the term "often" is purposeful; the "numbers" are not uniformly good, and in some of the cases

they are seriously off. Since DFT does not offer, as yet, a systematic way of improving one's result, this has led to a development of great many new functionals with partial and not always systematic improvements. We have remained with "numbers", which are often excellent in quality, but many a times we do not trust the results that we get, but we have no clear way of improving or testing these results with certitude. Nevertheless, even if the "numbers" are good or will some day become uniformly good, still we will be left with only "numbers". So where do we head now?

May be the tide is back and the quest of the pioneers of quantum chemistry for useful concepts and generalities has to resume its place in quantum chemistry. Only that now, this quest will be pursued with much better quantitative tools.⁷ Let's try then to make sense out of our "numbers" in this tutorial of chemical reactivity!

Chemical reactions consist of bond breaking and bond forming which lead to new molecules. Understanding what happens when molecules react and what governs the reaction surface, activation barrier, reaction mechanism, and reactivity patterns has been a principal goal of many theories/principles, as illustrated in the following cartoon, which lists on two "tablets" concepts/theories coming from physical organic/inorganic chemistry and from quantum chemistry. But as the "bewildered student" asks: what is the hierarchy of the different principles and the relationships between them? And which one(s) to obey first? As we shall try to show in this tutorial the Valence bond (VB) model can answer these questions and unify these concepts into a single coherent scheme.



1.2 Personalized History of Valence Bond Approach to Chemical Reactivity

As a young student of reactivity during my studies, I (SS) had always wanted to understand reactivity in some portable but unified way. In fact, the ability to understand the origins of barrier and to predict barrier heights from raw data is extremely useful and is a desirable feature of any general model of reactivity. In my first year as a Lecturer at Ben-Gurion University I completed the development of a VB model, which enabled me to consider both mechanisms and barrier heights.⁸ The first success was the S_N2 reaction, modeled with Addy Pross.^{9,10} Then I managed to gain a broader insight and did the same for other reaction types.¹¹⁻¹⁷ After teaming with Philippe Hiberty and subsequently with Wei Wu, we augmented the VB model by *ab-initio* VB calculations. These calculations pointed out that the semi-empirical VB predictions were basically correct.¹⁸⁻²³ Furthermore, having good quantitative “numbers” made it possible to derive expressions for the VB quantities

which matched VB computed values and enabled thereby making better predictions.^{14-17,23,24}

When I was joined by a sizeable group of young coworkers I always wished to teach them how to use the VB model. I finally had the opportunity to do this when the group started looking at enzymatic hydroxylation reactions that involve initial hydrogen abstraction by the enzymes. After some attempts we managed to cut through the viscous wade of the complexities of these metalloenzymes and model alkane hydroxylation reactions by usage of VB diagrams. We showed the root cause of why these reactions proceed preferentially in a stepwise manner, despite of the fact that the concerted oxygen insertion reaction has exceedingly favored thermodynamic driving force.^{16,25} Subsequently, the VB model was used to elucidate the reasons why sulfoxidation reactions were concerted, whereas olefin and arene epoxidation were stepwise like alkane hydroxylation.^{16,17,25-27} Subsequently, we managed to tune the model to a point where we could estimate barriers for HAT reactions,^{17,28} sulfoxidation,²⁶ and arene activation²⁷ for a variety of systems, and to develop the type of insight, which I felt was essential for a theory of chemical reactivity. We would like to share this insight in the present tutorial.

1.2.1. A Few Basics About VB Theory: Before we continue, the reader may wish to know “what is VB theory” and “what is the difference between it and the molecular orbital (MO) theory”? In a nutshell, VB theory describes the state wave function of a given chemical system as a linear combination of all the chemical structures that describe the distribution of the active electrons in the hybrid atomic orbitals (HAO) of those bonds that are being broken and made. In the simplest case of the H-H bond, the state wave function is given as a linear combination of a covalent structure, $\text{H}\cdot\text{---}\cdot\text{H}$, and two ionic structures, $\text{H}^+:\text{H}^-$ and $\text{H}:\text{H}^+$. If you were to run such calculations, you would find that the covalent structure dominates the wave function, having a weight of approximately 80% at the equilibrium bond distance.²⁹ Being chemists, however, we do not really need to run the calculations to know that the covalent structure should dominate the wave function. Still it is

nice to know that we can reason the calculations with such clarity. As we stretch the bond, gradually the weight of the ionic structures will dwindle until we reach a sufficiently long distance (say 3Å), where the VB wave function is completely described by the covalent structure such that at infinite distance we simply get two radicals. Again, as chemists, we understand that this must be the result of the calculations.

In MO theory, the same bond will be described by a doubly occupied σ orbital. But this compact description is insufficient because it corresponds to a wave function having 50% covalent and 50% ionic contributions. To correct this description, we must do configuration interaction (CI) calculations. Thus, by adding a configuration in which the electron pair occupies the antibonding σ^* MO, we get precisely the same wave function as the one obtained by VB theory. And further, as we stretch the H-H bond to a long distance, the two MO configurations (σ^2 and σ^{*2}) will attain the same contributions in the CI wave function, which now describes two radicals, precisely as in VB theory.²⁹ In MO terms, these results are not intuitively obvious. But by expansion of the MO wave function the equivalence of MO/CI and VB can be clearly proven.²⁹ So, the good news is that VB theory is equivalent to MO theory augmented by appropriate CI.

One additional feature I want to stress is the nature of the interaction of two electrons, which are not singlet-paired. Consider for example $\text{H}\cdot + \cdot\text{H}$ and let us not couple the spins of the two electrons to a singlet state, what will we get then? In VB theory, such an uncoupled electron duo is almost (75%) a triplet state.²⁹ In MO theory this will simply correspond to the $\sigma^1\sigma^{*1}$ triplet state. As we shall see later, it is beneficial to “travel” between these two conceptual worlds.⁷

As we cannot teach in the tutorial all the ingredients of VB theory and its relations to MO theory, here are some suggestions for further reading. A recent monograph²⁹ is recommended for learning the basics of VB theory (see chapters 2-4). Chapter 6 of the book describes the usage of VB diagrams for modeling and understanding chemical reactivity. Quantitative aspects of VB methodology have been recently reviewed.²⁴

Additionally there are a few review articles dedicated to VB modeling and chemical reactivity, and including many useful references.¹⁴⁻¹⁷ For applications of various VB theories (like generalized VB (GVB) theory, and spin-coupled VB (SCVB) theory) the reader may consult the additional references placed in the electronic supporting information (ESI) document. Accepting the advice of a referee, we also included in the ESI (see part III there) a short discussion, and relevant references, regarding the advantages of the VB approach over the FMO approach.

1.3. Introduction to the Tutorial Topic

In this tutorial review my coworkers and I focus on hydrogen atom transfer (HAT) reactivity, and then generalize to other reactions. HAT is one of the fundamental reactions occurring in nature and in oxidative chemistry. Most chemical oxidations begin with HAT. Cytochrome P450 and nonheme enzymes oxidize organic substrates often through HAT.^{16,17,30} Heme enzymes, e.g., HRP,³¹ build the cell walls in plants by initial HAT from phenols. Cell membranes are destroyed by HAT. DNA damage occurs by HAT. Proteins turn plaque by HAT. Production of Dopamine in our brains requires HAT. HAT occurs during combustion processes (see Ref. 17 and references therein). The endless list attests to the ubiquity and immense importance of HAT.

Our main goal in this tutorial is to achieve understanding of HAT reactivity going from the simplest hydrogen exchange reaction, $\text{H}^\bullet + \text{H}_2 \rightarrow \text{H}_2 + \text{H}^\bullet$, all the way to hydroxylation by Cytochrome P450 and what's in between. This will be done by usage of the VB diagram approach, which provides the tools to understand mechanisms and predict chemical reactivity patterns. Furthermore through VB modeling we illustrate the ways to estimate VB parameters from raw data and obtain thereby novel and general insight.

The tutorial will be based on recent reviews on HAT^{16,17} and papers on the relationship between HAT and proton-coupled electron transfer (PCET).^{28,32} Nevertheless, while the focus is on HAT reactivity, we would like also to provide the potential student of

this tutorial with the tools to consider other reactions^{14,15,26,27,33} as well, and project thereby the measure of unity brought about by the model. Since we took seriously our roles as tutors, our ESI document contains data that will help you improve your skills in applying the model. Yes, and once in a while we may address the reader as “you”, when we want to stress some issues needing self-tutoring.

2. The Fundamental VB Diagrams for Chemical Reactivity

2.1. Introducing Archetypical VB Correlation Diagrams

Let us introduce first the conceptual tools in Figure 1. These are a few archetypical VB state-crossing diagrams,^{14,15} which are based on *the principle of VB-structure correlations*, and which have been developed in 1981.⁸ The criterion of the correlation is *the chemical identity of the VB structures* in terms of electron-pairing and charges, etc.

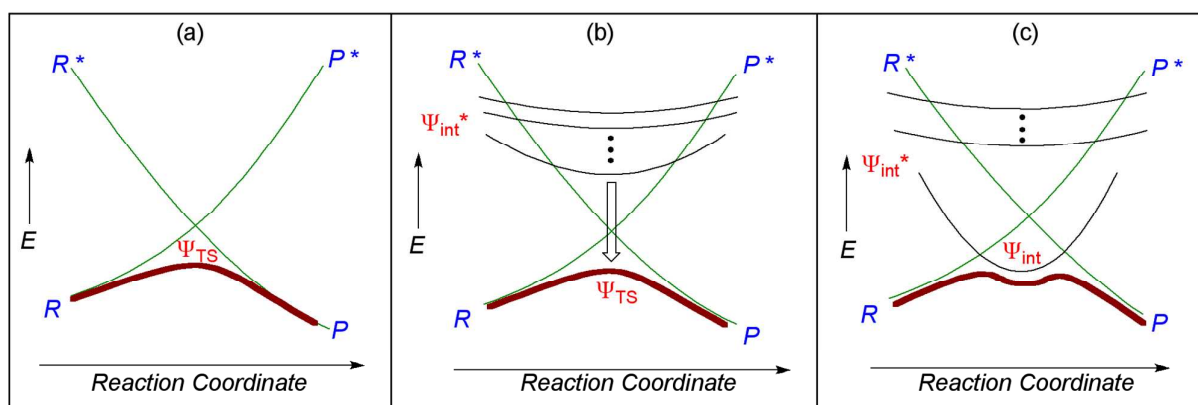


Figure 1. Archetypical VB diagrams: (a) A VBSCD showing two principal-state curves anchored in the ground states, R and P , of reactants and products, and in two corresponding promoted states, R^* and P^* . The state curves cross along the reaction coordinate and by mixing generate the curve in bold, which represents the energy profile for the thermal reaction with the corresponding transition state (TS). (b) A VBCMD showing the potential mixing of intermediate excited states, Ψ_{int}^* , into the TS, as implied by the arrow. (c) A VBCMD wherein one intermediate state crosses well below the crossing point of the principal curves, and the three-state mixing generates a stepwise mechanism with an intermediate, Ψ_{int} , separating R and P .

The first diagram in (a), which is called VB state-correlation diagram (VBSCD), displays two state curves of reactants (R) and products (P) that intersect, mix, and form thereby the barrier and the TS for an elementary process. The state-curves of the VBSCD have two ground states that correlate to two specific excited states, R^* and P^* . These

excited states *are electronic images (or templates)* of the ground states with which they correlate, and due to their relations to the ground states of R and P , these excited states are referred to as the “promoted states” of reactants and products. Thus, given a pair of R and P , we can immediately trace the two principal curves that involve the VB correlations of R to P^* and P to R^* .

Of course, besides the two promoted states of the principal state curves there exist many other excited states, which can affect chemical reactivity. The corresponding diagrams that contain more state curves than just the two principal curves, were named VB configuration mixing diagrams (VBCMD).^{10,14,15} In the usual situation, which is shown in Figure 1b, the intermediate-state curves will lie above the crossing point, and if sufficiently low in energy, it will mix into the TS of the two principal curves and lower its energy.

Figure 1c is an extreme VBCMD case where an intermediate state gets stabilized (by substitution, solvent, etc)^{11,13-16,29} and falls well below the crossing point of the principal state curves (e.g., triple ionic curves in S_N2 reactions, charge transfer states in Diels-Alder reactions of power electron acceptor dienophiles, like tetracyano-ethylene, the HAT curve in alkane hydroxylation by P450, and so on). Here, one intermediate-state curve crosses the two principal curves, and the three-state mixing *leads to a stepwise mechanism with an intermediate between R and P .*

As we shall see later, when we discuss e.g. PCET reactivity, some times the intermediate states will also be composed of two intersecting curves.^{17,28,32} What matters at this stage is to emphasize that the electronic structure of the intermediate-state curve is different than those of R and P .

Taken together the archetypal diagrams can model a gamut of reactivity patterns, and mechanisms in any desired reaction.

2.2. The Principle of Constructing the VBSCD

Figure 2a is a detailed version of Figure 1a. It is used as a template for defining the promoted states R^* and P^* for any given reaction type, and it will subsequently serve us to derive simple expressions for estimating the barriers. To exemplify the VBSCD construction, let us take a simple HAT reaction in which two radicals, X^\bullet and Y^\bullet , exchange between them an H atom, and construct the corresponding VBSCD in steps.²⁹ Later we shall derive a rule for a single shot construction of VBSCDs using the template in Figure 2a.

2.2.1. Detailed Construction of the VBSCD: In the first step in Figure 2b, we use only the two covalent structures of the interchanging bonds, $X^\bullet \text{H} \cdots \text{Y}$ and $\text{X} \cdots \text{H} \text{Y}^\bullet$. Thus, initially when the $\text{H} \cdots \text{Y}$ distance is short and the $\text{X} \cdots \text{H}$ is infinitely long, the covalent structure of the lower energy is $\text{X}^\bullet \text{H} \cdots \text{Y}$. Let us now follow this VB structure along the reaction coordinate. Thus, as we stretch the covalent $\text{H} \cdots \text{Y}$ bond the energy will go up. At the same time, bringing X^\bullet closer to H^\bullet , creates a triplet repulsion since the corresponding electrons are not paired to a singlet, and in fact maintain a triplet relationship.²⁹ This further raises the energy of the $\text{X}^\bullet \text{H} \cdots \text{Y}$ structure by virtue of Pauli repulsion. As the $\text{H} \cdots \text{Y}$ distance goes to infinity, while $\text{X} \cdots \text{H}$ shortens to the bond distance, the covalent $\text{H} \cdots \text{Y}$ bond gets completely broken, and triplet $\text{X}^\bullet \uparrow \uparrow \text{H}$ interaction is completely set. Thus, as can be seen from Figure 2b, the $\text{X}^\bullet \text{H} \cdots \text{Y}$ structure correlates along the reaction coordinate with an excited state where the $(\text{X}^\bullet \uparrow \uparrow \text{H})$ molecule is in a triplet state and this triplet state is coupled to a singlet pair between the H^\bullet and the infinitely distanced Y^\bullet radical. This long-distance pairing is indicated in Figure 2b by the arched lines connecting the electrons.

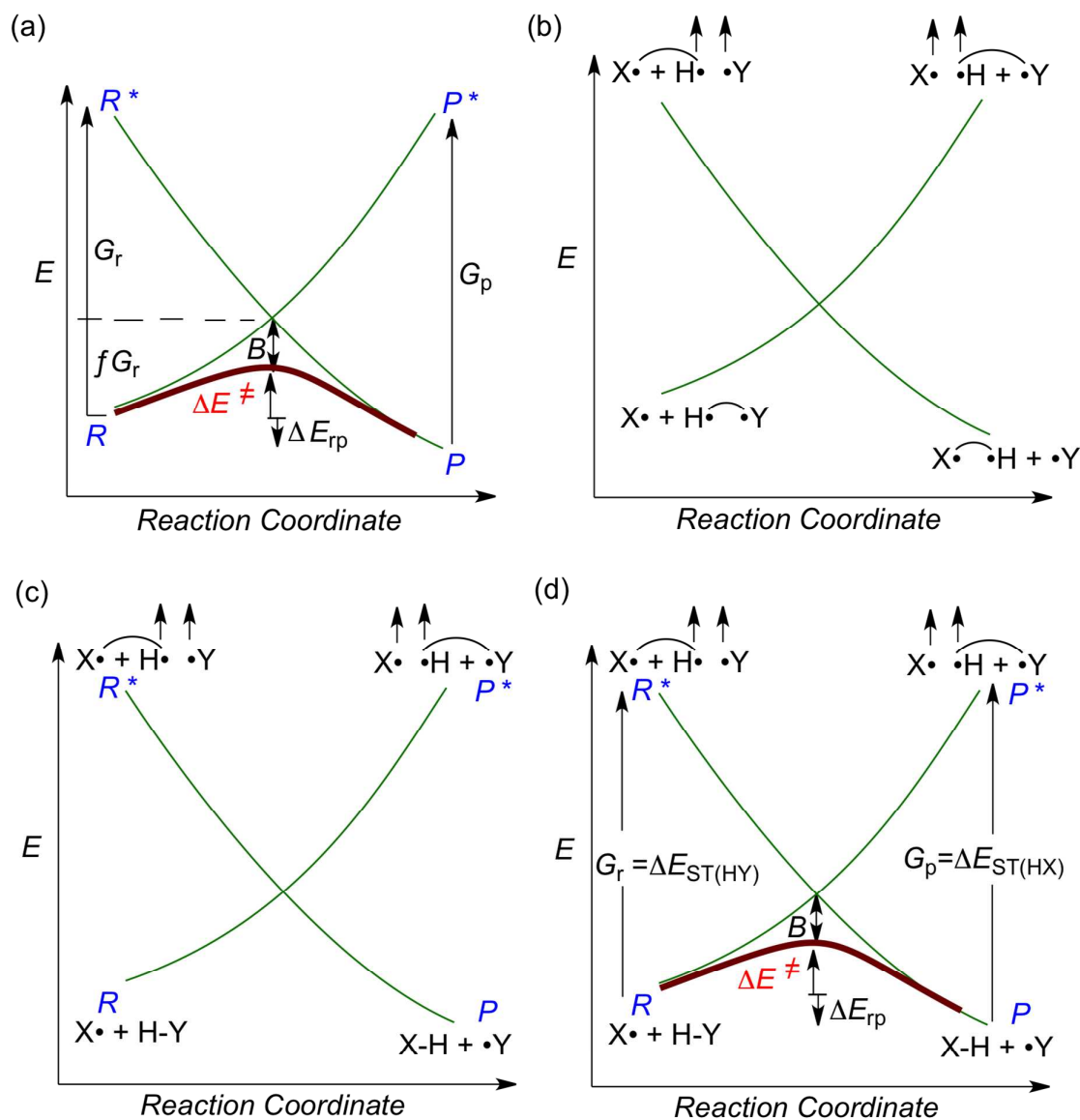


Figure 2. (a) Archetypical VBSCD diagram with the factors which determine the barrier, ΔE^\ddagger , for the reaction; the G 's are promotion energy gaps, B is the resonance energy of the TS, ΔE_{rp} is the thermodynamic driving force of the reaction, and fG_r is the height of the crossing point, relative to R , and expressed as a fraction f of the promotion gap at the reactant side, G_r . (b-d) Constructing the VBSCD diagram for hydrogen atom transfer reaction in three steps: (b) using only covalent structures, (c) allowing the covalent curves to mix in the ionic structures and become state curves, and (d) letting the state curves mix with one another and avoid the crossing. The resulting adiabatic state is shown by the thick curve, along with labels of the various energy quantities as in Figure 2a.

If we now consider the other end of the reaction coordinate where $X\cdots H$ is short and $H\cdots Y$ is infinitely long, then the lower VB structure is now the covalent structure of the products, $X\cdots H + Y\cdot$. If we follow the energy of this structure along the reverse reaction coordinate, it will correlate to an excited state wherein $(H\uparrow\uparrow Y)$ is in a triplet state, which is singlet-paired via the $H\cdot$ to the infinitely distanced $X\cdot$ radical as indicated by the arched lines connecting these electrons. In this manner we see that the two principal VB structures

of reactants and products *intersect along the reaction coordinate and correlate to specific excited states, which are their electronic images.*

We can further connect the energies of the curves and convert them to state curves, by allowing the ionic structures to mix into the curves we just created.²⁹ This is done in Figure 2c. For example, at the reactant geometry of the Figure, the ionic structures $X^+ (H^+ :Y^-)$ and $X^+ (H^- Y^+)$ will mix into the covalent structure, $X^+ H \cdots Y$, and will generate the reactant state R , in which the covalent $H \cdots Y$ structure becomes a full bond state $H-Y$ with covalent and ionic structures. Similarly, the ionic structures $(X^+ :H^-) Y^+$ and $(X^- H^+) Y^+$ will mix with the covalent state at the other end of the reaction coordinate, and will generate the product state P , having a full $X-H$ bond. On the other hand, the excited anchor points of the curves remain unchanged (recall the ionic structures do not mix when the singlet pair is infinitely separated) and serve as the promoted excited states, R^* and P^* , of the intersecting state curves. It is apparent that the spine of the diagram is the crossing of the covalent forms, while the mixing of the secondary ionic structures only modifies the energies and slopes of the state curves.

In the final stage in Figure 2d, we allow the two state curves to mix. Consequently, the state curves avoid the crossing and generate the adiabatic state (the thick curve), with a barrier and a transition state on the lower energy profile.

2.2.2. The Rule for Single Shot Construction of VBSCDs: Based on the above detailed construction of a VBSCD, the principle of constructing the promoted states for a chemical reaction can be summarized as in Rule 1:

Rule 1: In R^* we undo the electron pairing of those bonds in R that have to be broken during the $R \rightarrow P$ transformation, and we newly pair these electrons as in P . As such, R^* has the same electron pairing as P , but its geometry is identical to R . Therefore, as we move along the reaction coordinate in Figure 2, R^* is stabilized and correlates down to P . Similarly, on the other side, in P^* we un-pair the electrons of those bonds in P that have to

be broken during the reverse transformation, $P \rightarrow R$, and we newly pair these electrons as in R . Therefore, as we proceed along the reverse reaction coordinate in Figure 2, P^* will correlate down to R .

Rule 1 is applicable to any reaction. The literature involves a few sources with many examples of determining the identity of the promoted states.^{14,15,17,29} We shall practice this further below.

2.2.3. The Simple VBSCD Equation for the Barrier: The quantities G_r and G_p in Figure 2a are the corresponding promotion energies, due to this electron un-pairing and re-pairing, at the reactant and product sides, and are typical to the reaction in question, as we shall immediately see. The quantity B is the resonance energy of the transition state (TS) due to the VB mixing of the two states at their point of crossing. And finally, ΔE_{rp} is the thermodynamic “driving force” of the reaction. Figure 2a can be used also to derive barrier expressions involving the various quantities in the diagram.

The simplest barrier expression is:

$$\Delta E^\ddagger = fG_r - B \quad (1)$$

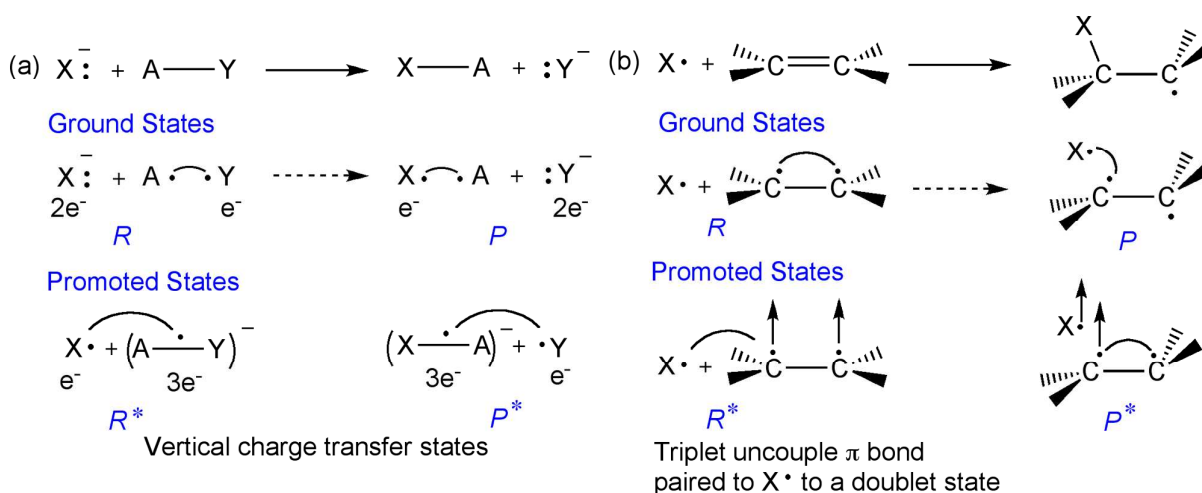
The term fG_r is the height of the crossing point relative to the reactant state R in Figure 2a. This quantity involves the distortion energy and repulsive interactions that cause the R state to rise in energy along the reaction coordinate and achieve resonance with P at the crossing point. Here, the two states mix and the TS is stabilized by the resonance energy B relative to the crossing point. The barrier is a balance between these two quantities.

The barrier expression in equation 1 is suitable primarily for series of reactions, which constitute “reaction families”, wherein f and B are constants or quasi-constants, such that relative reactivity is determined primarily by variations in G_r .^{14-16,29} As we shall see, G_r is

easy to estimate for a variety of reactions, and therefore eq. 1 is very effective for “reaction families”. This tutorial will attempt to teach you how this can be done for the specific example of HAT.

2.3. Generalized Promoted States and Promotion Energies in the VBSCD

The assignment of the promotion state for covalent or polar-covalent bonds reveals that there are two basic types of promotion energies: charge transfer- and triplet excitations. It is easy to see when do we need one of these excitation types, by writing down the reactants and products and partitioning the electrons between the atoms/fragments such that covalent bonds have equi-partition of one electron on each of the constituent fragments. Subsequently we count the electrons on the reacting atoms/fragments to see if any one lost an electron while another gained it. As illustrated in Scheme 1a for the S_N2 reaction, during the conversion of $X^- / A-Y$ to $X-A / Y^-$, X^- loses one electron and Y gains it. Hence, the R^* state that correlates to the product state P in the corresponding VBSCD is a charge transfer state, where the electron is taken from X^- and placed in the A-Y linkage. Symmetric arguments apply to the reverse reaction, where the P^* state will involve a vertical charge transfer state, when an electron from Y^- is transferred to X-A linkage.



Scheme 1. (a) Electron count for the S_N2 reaction showing that during the reaction X^- lost an electron to Y that became Y^- or vice versa in the reverse direction, Y^- loses and electron to X . The corresponding promoted states R^* or P^* are charge transfer states. (b) Electron count for the radical

addition reaction to a π -bond shows no redox change of the reaction centers. Hence, the promoted state R^* involve decoupling the electron pair of the π -bond to a triplet, while coupling one of the electrons to the radical X' to create a doublet state. Similarly P^* involves decoupling the electron pair of C-X bond to a triplet, and coupling one of the electrons to the radical C' to create a doublet state.

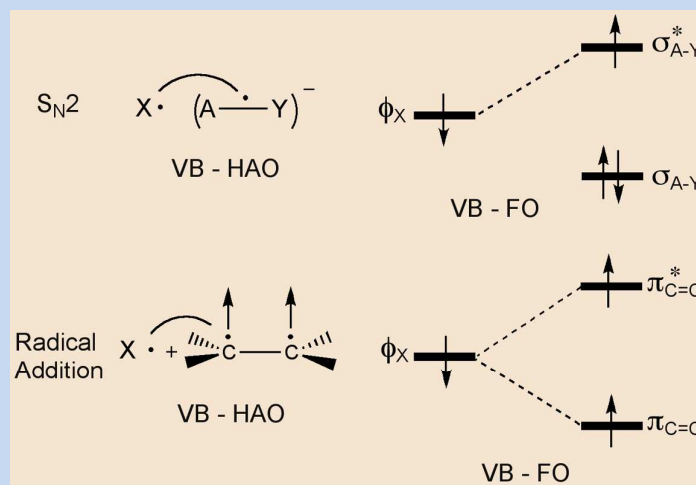
By contrast if we consider a radical addition to a double bond, in Scheme 1b, it is possible to see that each fragment keeps one electron in both R and P , without any redox change. Here the π -bond of the olefin undergoes decoupling of its electron pair to a triplet couple and the three electrons are re-coupled to the form that will lead to the product state P . We can express this description as Rule 2, which is more specific than Rule 1:

Rule 2: Whenever the oxidation numbers of the reacting fragments change during the reaction, the promoted states of the VBSCD will be charge transfer states. By contrast, if there is no change of oxidation numbers, then the promoted states involve a triplet decoupling of each of the bonds that breaks during the reaction, while pairing up the electrons across the bonds to be formed.

Note that it is perfectly possible and even beneficial to alternate back and forth between VB usages in terms of hybrid atomic orbitals (HAOs) and molecular orbital usages in terms of the fragment orbitals (FOs) of the reactants. **Textbox 1** shows the two alternative formulations.^{8,14,15,29}

Textbox 1: Equivalent Representations of the Promoted states

R^* can be equivalently represented either in terms of either hybrid atomic orbitals (HAOs) on the reaction centers to yield a VB-HAO cartoon, or by populating the electrons in the active fragment orbitals (FOs) of the reactants and generating a VB-FO representation. These alternative representations for R^* are depicted below for S_N2 and radical addition reactions. Note that in the VB-HAO representation the arched lines represent electrons that are paired to a singlet spin. In the VB-FO representation, dashed lines connecting the fragment orbitals represent the singlet-spin pairing of the corresponding electrons. For S_N2 , the singlet pair couples the ϕ_X - σ_{A-Y}^* electrons, while in radical addition the ϕ_X electron is coupled jointly to the triplet electrons in $\pi_{C=C}$ and $\pi_{C=C}^*$.



Usage of VB-FO orbital leads to a straightforward derivation of orbital symmetry rules.^{11,14,15,29} This is so even for odd-electron reactions, for which application of MO theory considerations (e.g., FMO theory, or orbital symmetry arguments) lead to ambiguous conclusions. The advantage of VB approach is that it covers everything FMO approach covers and adds many possibilities that are beyond FMO capabilities. This includes emergence of stepwise mechanisms, stereo selectivity and regio selectivity of odd electron reactions, change of nature of TS and intermediates in isoelectronic species (H_3 vs. Li_3 (also H_4 and H_6 vs. Li_4 and Li_6), H_3^- vs. X_3^- ($X = \text{halogen}$), CL_5^- vs. SiL_5^-).^{14,29} The interested reader may look at section III and the additional references in the ESI document.

If you wish to practice the VB-FO approach while you are reading this tutorial, you may try to construct the promoted states for a Diels Alder reaction, a 2+2 cycloaddition, carbene insertion, C-X bond activation by PdL₂, or any reaction you consider to be of interest to you. If you do so, you may discover for example, that the Woodward-Hoffmann rules are manifested in the resonance energy of the TS (*B*), and you will learn to make predictions about “facile forbidden reactions” and “almost impossible allowed ones”. The original literature^{11,14,15,29} will be helpful for this purpose.

2.4. Estimating VB parameters for the Simple VBSCD Equation

A key to a successful usage of the VBSCD is the ability to estimate the VB parameters *G*, *B* and *f*. Once these are known for a given reaction, the barrier becomes accessible too. So, let us proceed in this manner for HAT reactions.

2.4.1 Promotion Energies (*G*): It is possible to show by using semi-empirical VB theory that this triplet excitation of the bond (ΔE_{ST}) can be well approximated by twice the vertical bond energy, *D*.^{14,15,25} Since the VBSCD states *R** and *P** are vertical states (identical geometry as the ground state below), we have to use the vertical *D* values to estimate the promotion energies. Thus, the promotion gaps become:

$$G_r \approx 2D_{H-Y} \quad (2a)$$

$$G_p \approx 2D_{H-X} \quad (2b)$$

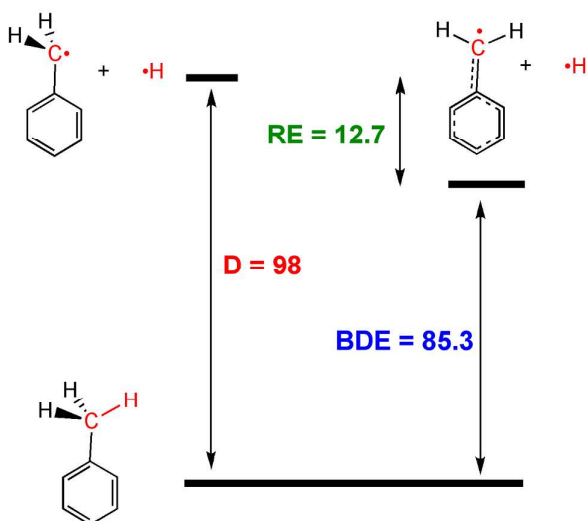


Figure 3. Pictorial representation for visualizing the difference between the vertical bond strength D and the bond dissociation energy BDE is exemplified for the C-H bond of toluene. RE is the reorganization energy of the benzyl radical. The values for D , BDE and RE are in kcal/mol.

Figure 3 shows the nature of the quantity D and its relationship to the more common and observable quantity, bond dissociation energy (BDE), using the C-H bond of toluene. It is seen that the vertical bond energy D involves the breakage of the C-H bond without relaxing the benzyl radical, so the latter remains pyramidal and its electron localized on the benzylic carbon. However, when we relax the benzyl radical, it becomes flat and delocalized and the bond energy taking us to this state is the BDE . The difference between D and BDE is the reorganization energy (RE) of the radical. Thus, for our HAT reactions we can write the following relations:

$$D_{\text{H-Y}} = BDE_{\text{H-Y}} + RE_{\text{Y}}. \quad (3a)$$

$$D_{\text{H-X}} = BDE_{\text{H-X}} + RE_{\text{X}}. \quad (3b)$$

Atomic radicals have $RE=0$, while polyatomic and delocalized radicals have large RE values,^{17,28} and as such, generally we have $D \geq BDE$. As seen later, the RE_{X} quantity is a key factor of the HAT barrier.

2.4.2. B and f Values: These two quantities are less easy to estimate in a general fashion. Nevertheless, by use of semi-empirical VB theory^{17,20} it is possible to relate the

resonance energy of the TS to the vertical bond strength at the TS geometry, namely to the D^\ddagger values.

For an identity reaction where $X=Y$, $B=\frac{1}{2}D_{X-H}^\ddagger$, and for nonidentity reactions $B=\frac{1}{4}[D_{Y-H}^\ddagger + D_{X-H}^\ddagger]$, namely it is one half of the average D^\ddagger value in the $X\cdots H\cdots Y$ TS species. Since the $H\cdots Y$ and $H\cdots X$ bonds of the TS are longer than in the relaxed molecules, the D^\ddagger values at the TS are smaller than the D values for the ground state molecules. Therefore, by careful benchmarking against *ab-initio* VB calculations, we found it reasonably accurate to estimate B by usage of the BDE values, which are smaller than the D values. Thus, to apply the simple barrier equation we can estimate the resonance energy for $X\cdots H\cdots Y$ TS using the following expression:

$$B(X\cdots H\cdots Y) = \frac{1}{4}[BDE_{Y-H} + BDE_{X-H}] \quad (4)$$

Since the weaker of the two bonds is less stretched in the TS, we found^{20,23} that BDE_w , i.e., the BDE of the weaker bond often dominates the sum in eq. 4. Thus, B is simplified as

$$B(X\cdots H\cdots Y) \sim \frac{1}{2} BDE_w \quad (5)$$

Finally the f factors were shown by semi-empirical VB theory^{17,20} to be:

$$f = 0.3 \text{ to } 1/3 \quad (6)$$

We are now practically ready to apply the simple barrier equation to HAT reaction families. It is apparent that in principle the equation enables us to estimate barriers from raw data such as D , BDE and RE .

3. VB Modeling of HAT and Other Reactions in Cytochrome

P450:

3.1 HAT reaction by Cytochrome P450: Estimating Barriers with the Simple VBSCD Equation

We are going to start with a reaction that seems quite complex, the HAT step and the rate-determining step of alkane hydroxylation by the enzyme cytochrome P450. The active species of P450, so called Compound I (Cpd I), is shown in Figure 4a, and is seen to involve a high-valent iron(IV)-oxo porphyrin radical-cation species (see **Textbox 2**). Without going too deeply into VB theory or any other theory, simply calculating Cpd I with density functional theory and inspecting the spin distribution (Figure 4a), reveals that the oxo center is a radical center and it can participate in a simple HAT.

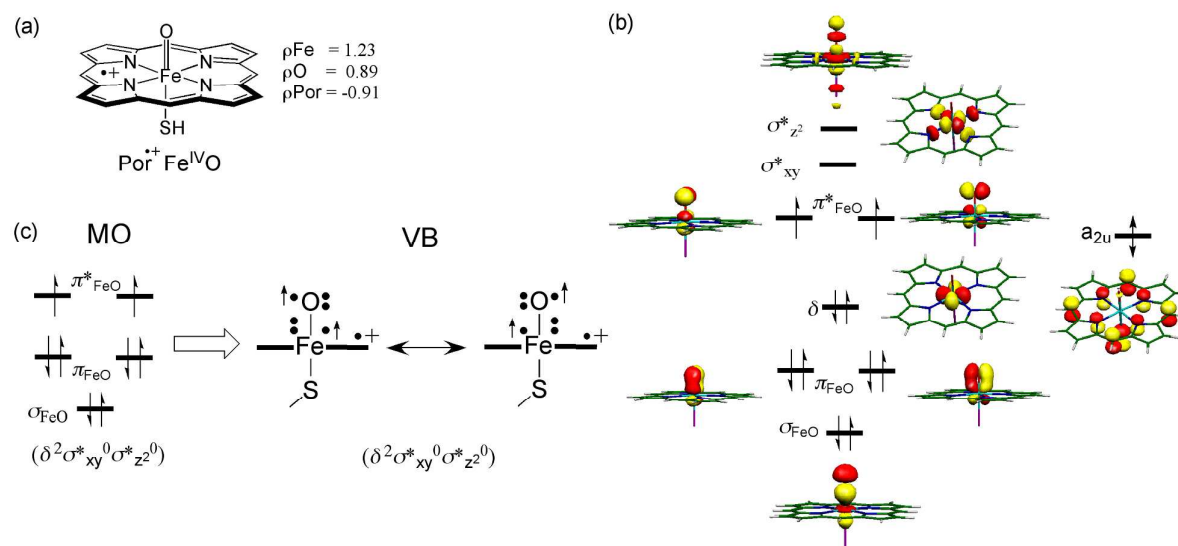


Figure 4. (a) Compound I (Cpd I) and its spin densities (ρ) on Por, Fe, and O (calculated with B3LYP/LACVP). (b) The MO diagram for Cpd I, showing in addition to the five d-type orbitals (δ , π^*_{FeO} , σ^*_{xy} , $\sigma^*_{z^2}$) also the doubly occupied π_{FeO} orbitals in two perpendicular planes, as well as the σ_{FeO} orbital. Note that the single electron in the a_{2u} orbital of porphyrin can assume spin up or spin down orientations, leading to quartet and doublet spin states. (c) The equivalence of the MO and VB representations; the latter shows clearly the diradical character with an oxo radical center. Note that two heavy bars flanking iron represent the porphyrin ring. Reproduced from Figure 2 of Ref. 16 with permission from American Chemical Society

This radical character of the oxo ligand of Cpd I can be derived from the electronic structure, using either the MO occupation diagram in (b) or the equivalent VB picture in (c). Thus, the MO diagram reveals that the iron(IV)-oxo moiety has $\pi^2 \pi^{*1}$ occupancy in the two

perpendicular sets of π -type MOs, and is hence an analog of the ${}^3\text{O}_2$ molecule,^{16,34-36} having therefore a diradical character with an unpaired electron on the oxygen. Similarly, in (c) we show the equivalent VB picture, where the $\pi^2 \pi^{*1}$ configuration of the two sets of π -type MOs corresponds to two resonating 3-electron bonds^{29,36} in the VB representation. Clearly, in any one of the representations, the FeO moiety is a diradical, *with an oxo radical center*.

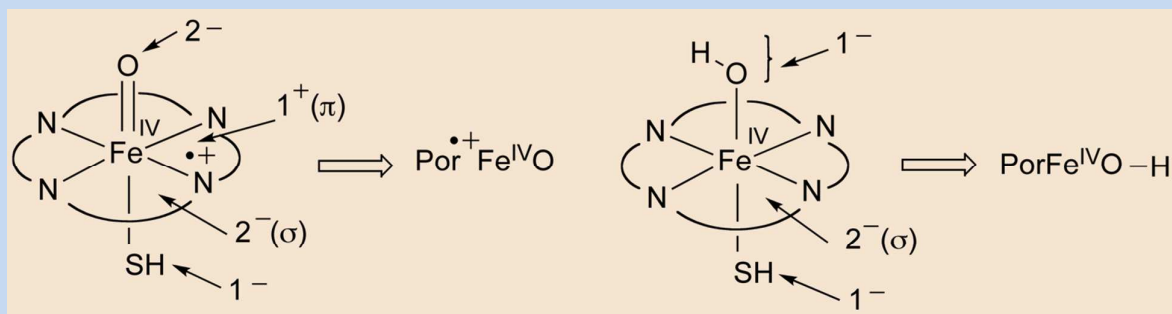
An additional feature in Figure 4b to be mentioned is that Cpd I possesses also an additional unpaired electron in the porphyrin orbital, labeled a_{2u} . This generates therefore two close energy states, with doublet (when the a_{2u} electron has spin down) and quartet (when the a_{2u} electron has spin up) spins. This is the basis of two-state reactivity (TSR) in P450.³⁶ During H-abstraction the two states are very close in energy, and therefore we shall not discuss the spin-state issue and we shall make use of the average HAT barrier for the two states. The TSR reactivity patterns transpire the subsequent step of radical rebound to form the ferric alcohol complex.^{16,17,25,30}

Textbox 2: On the Oxidation State Formalism

The oxidation number formalism in inorganic chemistry assigns octet to all the ligand, and appropriates electrons from the transition metal to fill the valence-shell of the ligands.

Thus, as shown for Cpd I below, the oxo has an oxidation number of 2-, the thiolate ligand is 1-, the porphyrin is 2- in the σ component and 1+ in the π component. Since Cpd I is neutral, the oxidation number on iron is IV, and taken together Cpd I is represented as $\text{Por}^{\bullet+}\text{Fe(IV)O}$.

After H-abstraction by Cpd I, the OH group has an oxidation number of 1-, the SH is 1-, and the porphyrin is 2- (σ component), since the intermediate is neutral, the oxidation number of Fe is IV, while the porphyrin has gained an electron into its π -electronic component. Taken together, we have PorFe(IV)OH , as shown in the corresponding drawing below. The R^* state in the corresponding VBSCD (Fig. 6) will have spin pairing across O and H and will therefore have precisely the same oxidation numbers as the $\text{PorFe}^{\text{IV}}\text{OH}$ species.



Where is the gained electron coming from in $\text{PorFe}^{\text{IV}}\text{OH}$? Thus, in $\text{Por}^{\bullet+}\text{Fe}^{\text{IV}}\text{O}$ the oxo is O^{2-} , while the HO moiety is HO^{1-} ; which means that the O^{2-} returned one electron to the porphyrin and the O^{1-} coupled with H^{\bullet} . For more detailed discussions consult the original literature.^{16,30}

In order to demonstrate the usage of the VB model, we collected in Figure 5 a variety of alkanes that undergo HAT with Cpd I. Near each alkane we display three numbers, $\Delta E_{\text{av}}^{\ddagger}/D_{\text{C-H}}(BDE_{\text{C-H}})$, which are the spin-state averaged barriers followed by the bond strength $D_{\text{C-H}}$ and the bond dissociation energy $BDE_{\text{C-H}}$. All quantities are computed with density functional theory (DFT) using the hybrid functional B3LYP.¹⁶ The data in Table S1 will help you self-tutor yourself.

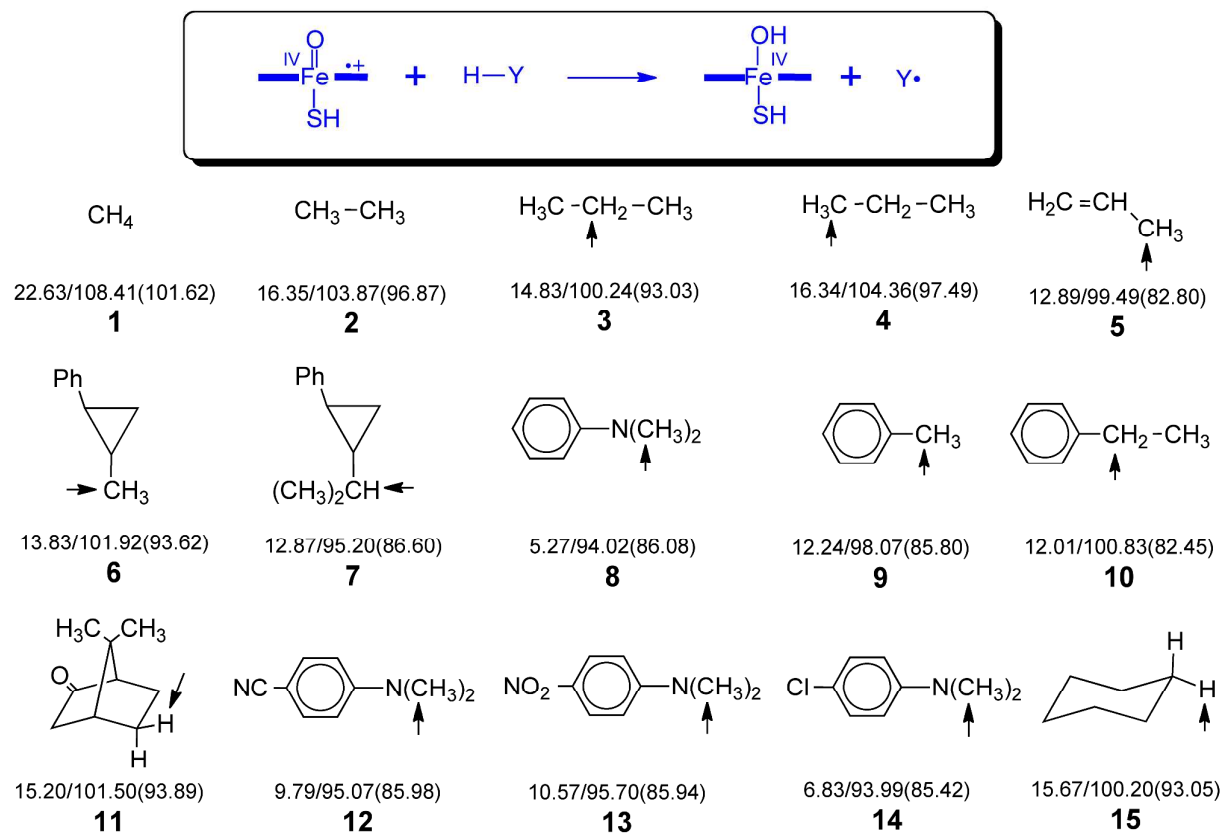


Figure 5. Alkanes **1-15** and computed DFT data (in kcal/mol), shown as $\Delta E_{\text{av}}^{\ddagger}/D_{\text{CH}}(BDE_{\text{CH}})$. $\Delta E_{\text{av}}^{\ddagger}$ are spin-state averaged barriers, here and elsewhere calculated with a triple- ζ polarized basis-set with zero point energy (ZPE) correction. The BDE_{OH} value for Cpd **1** is 89.28 kcal/mol. Reproduced from Figure 7 of Ref. 16 with permission from American Chemical Society

The corresponding VBSCD is shown in Figure 6, where we follow the oxidation number notations. Thus, in the promoted state, the oxo radical is singlet paired with the H• of the triplet-promoted alkane. Since the oxidation number of the “OH” group is 1- the heme oxidation state is decreased from $\text{Por}^{\bullet+}\text{Fe}^{\text{IV}}\text{O}$ to $\text{PorFe}^{\text{IV}}\text{O}\cdot\text{—}\cdot\text{H}$ (**Textbox 2**).

The G_r quantity in the VBSCD in Figure 6 is $2D_{\text{H-Y}}$, which is easily available. But we still need to quantify f and B . We have an initial estimate for B recalling the semi-empirical relation in eq. 5 above, $B \sim \frac{1}{2}BDE_w$, where BDE_w is the BDE of the weaker of the two bonds, H-Y/H-O, which interchange during the reaction. For the data set displayed in Figure 5 these B values range between 41 and 45 kcal/mol. The semi-empirical estimate of f is 0.3 to 1/3 (equation 6). These values give us a lead.

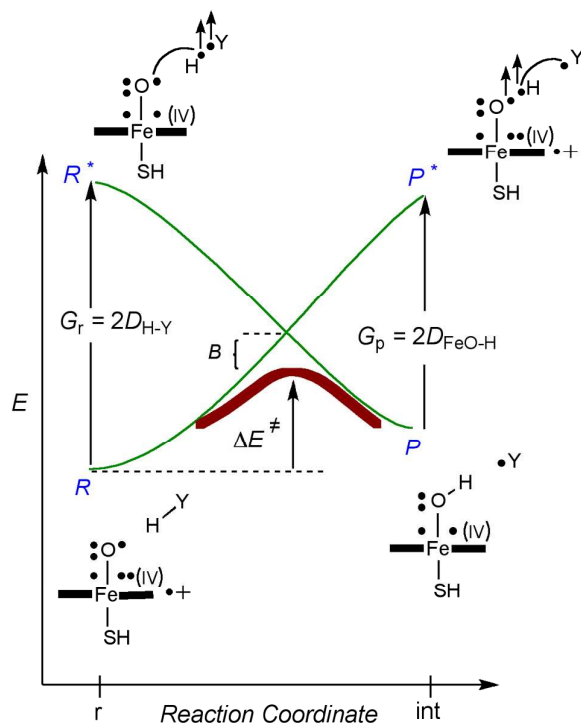


Figure 6. The VBSCD for the HAT process in which Cpd I abstracts an H atom from an alkane H-Y.

What we usually do first is to test if the f and B quantities of the reaction series at hand are anywhere close to the above semi-empirical estimates. Thus, we use $f = 0.3$ and find the B values that are required to reproduce the barriers. Subsequently, we use an average of these B values and find the f values needed to reproduce the barriers. The f values we find for the data set in Figure 5 cluster around 0.30, close to the semi-empirical value, while the average B value is around 47 kcal/mol, again in the ballpark of the semi-empirical estimates. To avoid seeking individual f and B values for every reaction, we consider the reaction at hand as a “reaction family” having common f and B values, and we seek values which are close to these averages and which provide the smallest deviation from the DFT barriers. For the data set in Figure 5 these barriers follow from equation 7:

$$\Delta E_{\text{VB}}^{\ddagger} = 0.6D_{\text{CH}} - 46.78 \text{ (kcal/mol)}; (G_r = 2D_{\text{H-Y}} = 2D_{\text{CH}}) \quad (7)$$

Figure 7 displays the correlation of the so-estimated VB barriers vs. the DFT computed barriers. The entire data set has $R^2 = 0.834$. Importantly, excluding the alkanes **1**, **8**, and **14**, which deviate the most from the DFT barriers produces a set of VB barriers with a mean deviation of ± 0.90 kcal/mol compared with DFT values (Figure 5).

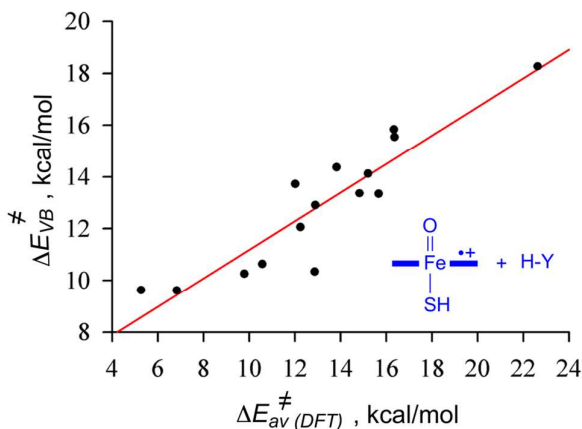


Figure 7. VB barriers (eq. 7) plotted against spin-state averaged DFT barriers. Reproduced from Figure 8 of Ref. 16 with permission from American Chemical Society

It turns out that the deviation of **1** originated in the convergence of the original DFT calculations²⁵ on a higher TS wherein the iron center is in the Fe(III) state, whereas the lowest TS with Fe(IV) has a spin-state averaged barrier of 19.1 kcal/mol,³⁷ which is very close to $\Delta E_{VB}^{\ddagger} = 18.3$ kcal/mol predicted by the model in equation 6. In the original literature¹⁶ we also explained the physical basis for the deviations of **8** and **14**; these are the best electron donors among the alkanes in Figure 5, and line in the VBSCD in Figure 1b, there is a charge transfer-state curve that mixes into the TS and lowers its barrier by increasing its resonance energy B (see later such a case). As such, eq. 7 appears to predict quite well the computed barriers, and the series behave by and large as “a reaction family” with relatively small scatters in the f and B quantities. The larger deviations have a physical basis in additional mixing through the charge transfer state.

3.2 Other Reactions of Cytochrome P450

Many reaction series that you will encounter constitute reaction families. As such, our advice is to always start with the simple equation of the barrier and try to model the barrier

data. As a reader of this tutorial, it might come handy to screen the original literature^{14-16,26,27} and reconstruct some of these series for other reaction types. Among these are reactions of electrophile-nucleophile pairs, in organic chemistry and in P450. In all these cases, the barriers obey the simple equation:

$$\Delta E_{\text{VB}}^{\ddagger} = f G_{\text{CT}} - B \quad (8a)$$

where G_{CT} is the charge transfer promotion energy. For example, in sulfoxidation of substituted thioethers by Cpd I of P450,¹⁶ the series is a perfect reaction family with $f = 0.2$ and $B = 14$ kcal/mol, which typify reactions of electrophiles and nucleophiles.

A very interesting case is the dual reactivity³⁸ we analyzed for arene activation by Cpd I of P450.²⁷ The activation step involves a radical attack of the oxo radical of Cpd I on the arene to form a Meisenheimer complex. The promotion energy gap G_r for this step is the singlet-triplet excitation, ΔE_{ST} , of the arene, which is required to decouple two of the π -electrons. But, much like the case of the deviant alkanes discussed above for HAT, here too, there is a low-lying charge transfer state that mixes into the TS and increases its resonance energy, B (Figure S1). Since the mixing of the charge transfer state depends on its relative energy to the covalent state-curves, then the smaller the ionization potential of the arene (IP_{ArX}) the larger the B value is expected to be. Accordingly, one can estimate barriers using equation 8, which shows a dual dependence of the barriers, on the promotion gap ΔE_{ST} and on the factor B that varies in proportion to the inverse of IP_{ArX} :

$$\Delta E_{\text{VB}}^{\ddagger} = f \Delta E_{\text{ST}} - B; f = 0.3, B = B(1/IP_{\text{ArX}}), G = \Delta E_{\text{ST}} \quad (8b)$$

Figure 8 shows the correlation of the so estimated VB barriers with the corresponding DFT barriers, for a variety of substituted arenes activated by Cpd I of P450 (see Table S1). Although the correlation is not perfect ($R^2 = 0.87$), it is still remarkable considering the

variety of arenes. It shows that the VB model is capable of estimating barriers from raw data.

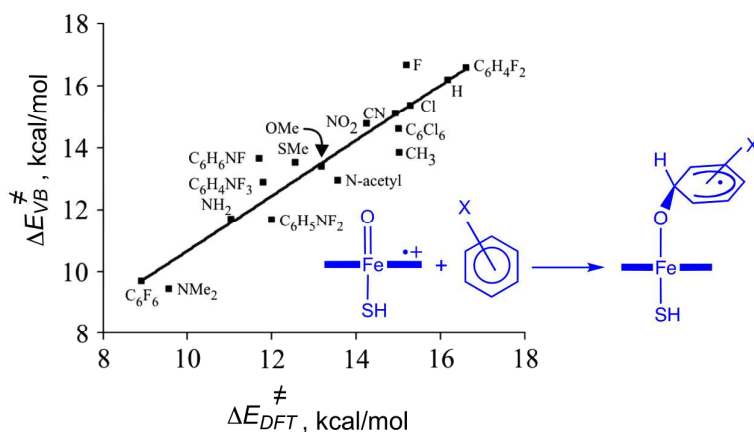


Figure 8. Estimated VB barriers using the expression, $\Delta E_{VB}^{\ddagger} = 0.3\Delta E_{ST} - B$; $B = B(1/IP_{ArX})$, and their correlation with corresponding DFT barriers for arene activation by Cpd I. $B(1/IP_{ArX})$ indicates that B is proportional to the inverse of IP_{ArX} .

Olefin activation by P450 exhibits the same dual dependence as arene activation; on ΔE_{ST} of the olefin and its IP value.³³ Figure 9a shows the full VB diagram for olefin epoxidation by Cpd I. This is a VBCMD of the general type in Figure 1c. The C=C bond activation involves the avoided crossing of the reactant state R with an intermediate state, $\Psi_{int}^*(Fe^{IV})$, which leads to the radical intermediate in the middle of the diagram. Subsequently, the intermediate state is crossed by the R^* state, during the ring closure to the epoxide product. Note that the R^* state is a charge transfer state, Ψ_{CT} , generated by an electron transfer from the olefin to Cpd I. It is expected that this charge transfer state will mix into the TS for bond activation, TS_{BA} , and thereby increase its resonance energy, in a manner that depends on the inverse value of the ionization potential of the olefin (IP_O). Thus, the C=C bond activation may behave in an analogous manner to arene activation, and obey the same barrier expression (eq. 8). To test this notion, we estimated the corresponding VB barriers for the recently studied olefin activations by Cpd I.³³ The raw data is collected in the Table S2. Figure 9b shows the plot of the VB barriers against the corresponding DFT barriers for all the arenes in Figure 8 and the olefins using a unified barrier equation as eq. 8. The correlation deteriorates of course by adding the olefin data,

but it is still apparent ($R^2 = 0.828$), and it basically shows that it is possible to unify arene and olefin activations in a single expression that predicts their barriers from raw data.

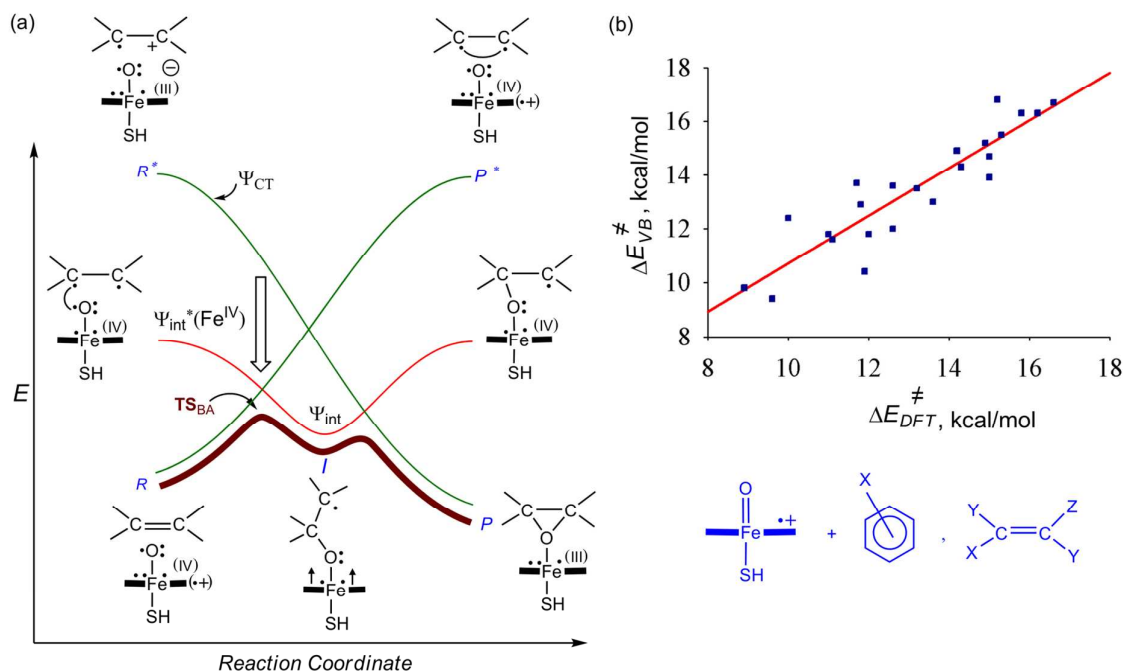


Figure 9. (a) The VBCMD for olefin epoxidation by P450 Cpd I. The first and rate-determining step involves a radical attack of the oxo of Cpd I on the π -C=C bond to yield a radical intermediate. The heavy arrow indicates that the charge transfer state, Ψ_{CT} , mixes into the transition state for bond activation (TS_{BA}). (b) A Plot of VB estimated barrier using the expression $\Delta E_{VB}^{\ddagger} = 0.3\Delta E_{ST} - B$; $B = B(1/IP)$, where all the arenes from Figure 8 as well as the olefin data are included.

3.3. Estimating HAT Barriers with the Explicit VBSCD Equation

What we did in the previous section requires a bit of experience in carefully deducing the values of B and f of the reaction family. What we would like to do now is something more ambitious. We would like to predict the barriers of the HAT reactions in Figure 10a,b, which involves 45 HAT processes starting from $H + H_2$ and going all the way to the P450 cases we considered above in Figure 5 and some new ones, with combinations of identity and non-identity reactions.

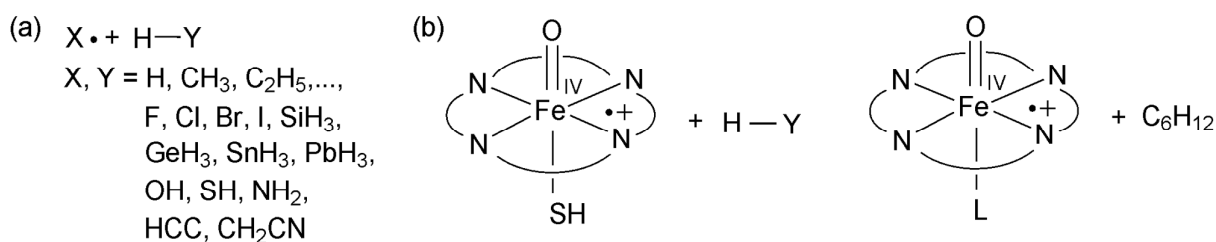


Figure 10. (a) 28 Different HAT reactions $X\cdot + H-Y$ with all possible combinations of X and Y fragments, including $X=Y$ and $X\neq Y$. (b) HAT reactions of Cpd I by P450 (for alkanes (H-Y) see Figure 5), and by models of Cpd I with different axial ligand (SH, Cl, OAc, CF_3SO_3) reacting with C_6H_{12} .

It is apparent that with this variable data set we cannot actually have a constant B . We must therefore use the explicit equation for the barrier, that allows estimating also f and B for individual cases. Such a more complex equation is the following expression

$$\Delta E^\ddagger = f_0 G_0 + \frac{1}{2} \Delta E_{rp} + \frac{1}{2} \Delta E_{rp}^2 / G_0 - B \quad (9)$$

This expression considers explicitly the two promotion gaps and f factors through their average values, G_0 , and f_0 , as well as the thermodynamic driving force ΔE_{rp} . Details of this derivation can be found in the original papers.^{20,23,29}

In equation 9, G_0 is the average promotion gap and f_0 is the average fraction factor and is given as:

$$G_0 = \frac{1}{2} [G_r + G_p] = [D_{H-Y} + D_{X-H}] \quad (10)$$

$$f_0 = \frac{1}{2} [f_r + f_p] = 0.3 \quad (11)$$

The resonance energy B is given by one half of the average BDE's:

$$B = \frac{1}{4} [BDE_{H-Y} + BDE_{X-H}] \quad (12)$$

And the thermodynamic driving force is given as the BDE difference:

$$\Delta E_{rp} = BDE_{H-Y} - BDE_{X-H} \quad (13)$$

Using the above relationships, equation 9 becomes then the following expression for the barrier:

$$\Delta E_{\text{VB}}^{\ddagger} = 0.3(D_{\text{H-Y}} + D_{\text{X-H}}) + \frac{1}{2}(BDE_{\text{H-Y}} - BDE_{\text{X-H}}) + \frac{1}{2}(BDE_{\text{H-Y}} - BDE_{\text{X-H}})^2 / (D_{\text{H-Y}} + D_{\text{X-H}}) - \frac{1}{4}[BDE_{\text{H-Y}} + BDE_{\text{X-H}}] \quad (14)$$

Here we left all the terms in the order they appear in eq. 9 so as to ease the comparison of the two equations. The reference barriers are computed with CCSD(T) with a complete basis set (CBS) limit, for all the cases in Figure 10a, and with DFT (B3LYP with a triple zeta basis set) for the P450 cases in Figure 10b. The correlation of the so-predicted VB barriers vis-à-vis the reference barrier is shown in Figure 11 using two different barrier equations; the one labelled as $\Delta E_{\text{VB}}^{\ddagger}(1)$ omits the quadratic term in eq. 14, and the other labelled as $\Delta E_{\text{VB}}^{\ddagger}(9)$ includes the quadratic term.

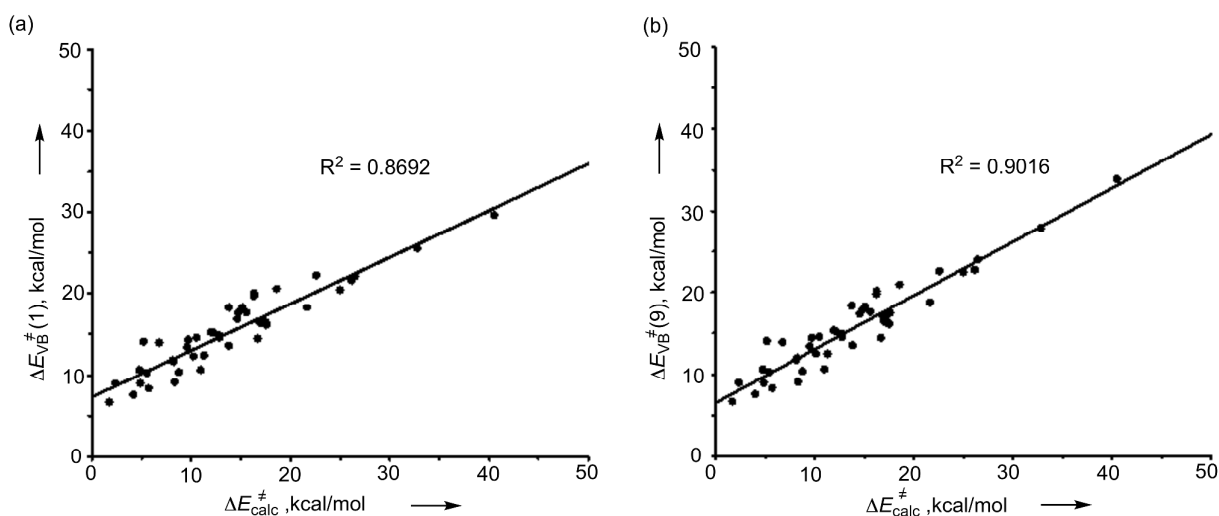


Figure 11. Plots of VB barriers against corresponding reference barriers (CCSD(T)/CBS; B3LYP/triple-zeta): (a) For $\Delta E_{\text{VB}}^{\ddagger}(1)$ values, obtained by omitting the quadrating term from equation 9. (b) For $\Delta E_{\text{VB}}^{\ddagger}(9)$ values, obtained with the quadratic term included. Adapted with permission from Figure 2 in ref. 17.

It is apparent that the present data set the full equation with the quadratic term retained (in b) is better than the truncated one (in a). The correlation coefficients in Figure 11 are not too bad for such a large data set with variable theoretical methods. Furthermore, if we remove the P450 data, the correlation coefficients improves up to $R^2 = 0.967$ (see Figure S3). This is no wonder since the first set involves CCSD(T)/CBS data while the P450 set is calculated with DFT. Still it is important to recognize that the *BDE* and *D* values

in equations 10-14 are variables that represent the promotion gap and other quantities in the VB equation, and as such, the equation will produce barriers that are gauged by the particular values of the variables, irrespective of their method of determination. It is therefore perfectly legitimate to use the entire set of data *vis-à-vis* the VB predictions. Clearly, while the correlation coefficient in Figure 11b is not perfect, still considering the range of reactions, it is fair to say that the VBSCD model captures the essence of the HAT barrier variation across the board. The fact that model can predict barriers from raw data is a powerful conclusion that emerges from the VB modelling.

All the D , BDE , RE_X , (RE_Y), and barrier data are given in the ESI (see Table S3-S5), and we again recommend anyone who wishes to benefit from the tutorial to use these data and reconstruct Figure 11.

4. Insight into Key Factors of the HAT Barrier

4.1. Identity HAT Reactions

Having demonstrated that the model can predict HAT barriers from raw data, we wish now to try and extract insight from the numbers. In order not to complicate the discussion we begin with identity reactions, $X\cdot + H-X \rightarrow X-H + \cdot X$, and use the VBSCD in Figure 12.

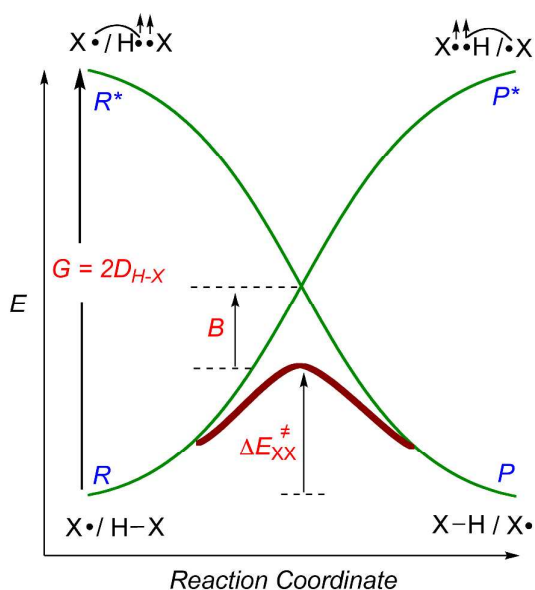


Figure 12. A VBSCD for a general identity reaction, $X\cdot + H-X \rightarrow X-H + \cdot X$. Reproduced from Ref. 28 with permission of The Royal Society of Chemistry.

Setting D_{H-X} equal to D_{H-Y} and the same for the corresponding BDE_{H-X} and BDE_{H-Y} quantities in the barrier equation 14, we get the following compact expression for the barrier:

$$\Delta E_{VB,XX}^\ddagger = 0.6D_{H-X} - 0.5BDE_{H-X} \quad (15)$$

Since $D_{H-X} = BDE_{H-X} + RE_{X\cdot}$, we can plug this into equation 15 and obtain the following attractive expression:

$$\Delta E_{VB,XX}^\ddagger = 0.1BDE_{H-X} + 0.6RE_{X\cdot} \quad (16)$$

Thus, the identity barrier is seen to depend weakly on the BDE of the bond being broken and to have a strong dependence on the reorganization energy of the radical $X\cdot$. We recall from Figure 3 that $RE_{X\cdot}$ is the energy required to distort the $X\cdot$ radical and to localize its electron on the atom center that is bonded to H in the X-H molecule.

To appreciate the role of $RE_{X\cdot}$, turn to Table 1. The Table shows a variety of identity HAT reactions along with the corresponding BDE_{H-X} and $RE_{X\cdot}$ quantities, the barrier determined with the VB equation 15, and reference barriers; some of the reference barriers are experimentally determined, others are determined by CCSD(T)/CBS and/or DFT. All these data appears in the original literature.^{17,28}

Table 1. BDE and $RE_{X\cdot}$ data (kcal/mol) and corresponding VB-derived barriers (kcal/mol) shown along with reference barriers: Experimental, CCSD(T)/CBS, and other calculated barriers for identity HAT reactions, $X\cdot + H-X \rightarrow X-H + \cdot X$.

Entry	X	$BDE^{[a]}$	$RE_{X\cdot}$	$\Delta E_{VB,XX}^\ddagger$	$\Delta E_{CCSD(T)/CBS}^\ddagger$	ΔE_{exp}^\ddagger	$\Delta E^\ddagger(\text{others})^{[g]}$
1	H	103.2	0.0	10.3	8.8	9.7 ^[d]	
2	CH ₃	103.2	6.8	14.4	16.7	14.9 ^[d]	
3	C ₂ H ₅ ^[a]	96.9	7.0	13.9			14.3 ^[f]
4	HCC	132.9	0.1	13.4	9.6		12.8 ^[f]
5	NCCH ₂	95.7	10.8	16.0	17.6		
6	PhCH ₂ ^[a]	85.8 ^[a]	12.3 ^[a]	15.9		19.9±2.2 ^[e] (18.7±2.2)	16.5 ^[a]
7	F	135.1	0.0	13.5	13.9		
8	OH	117.0	0.0	11.7	8.2	4.2 ^[f]	[7.8](4.15)7.3 ^[h]
9	NH ₂	105.3	0.1	10.6	11.0		
10	Allyl ^[a]	82.6	16.9	18.4			19.4 ^[a]

11	C ₆ H ₇ ^[a,b]	69.5	20.4	19.2	20.6 ^[a]
12	C ₁₄ H ₁₁ ^[a,c]	72.8	15.4	16.5	17.2 ^[a]

^[a] These cases were computed with DFT. Entries 1-6 are from Ref. 17, entries 10-12 from Ref. 28. ^[b]This is the cyclohexenyl radical derived from 1,4-cyclohexadiene. ^[c]This is the radical derived by H-abstraction from 9,10-dihydroanthracene ^[d]See Ref. 17. ^[e]Experimental E_a value. In parentheses is a ΔH^\ddagger value estimated from E_a . See Ref. 17. ^[f]Experimental data; see Ref. 17. ^[g]Unless indicated otherwise, these are computational data cited in Ref.17. ^[h]The value in brackets is an activation barrier without ZPE-correction, the value in parentheses is the estimated activation barrier including the tunneling factor. The last value is the ZPE corrected barrier. Data cited in Ref. 17.

Inspection of the column of $\Delta E_{VB,XX}^\ddagger$ values by comparison to the columns of the reference barriers shows that all in all, the predictions of equation 16 are good. It captures the essence of the identity barrier, using raw data.

An interesting comparison is the H[•]/H₂ and H₃C[•]/CH₄ exchanges in entries 1 and 2. The BDE s of H-H and C-H are seen to be essentially identical and nevertheless, the barrier for the second reaction is significantly larger than of the first reaction. The reason is seen to be the RE_X quantity: H[•] is a monoatomic radical and its reorganization energy is zero, while H₃C[•] is a polyatomic radical which is flat when free, and has to undergo significant pyramidalization to make a C-H bond. It is the significant RE_{CH_3} quantity that dominates the barrier difference and the root cause for the higher barrier for the H₃C[•]/CH₄ exchange.

Consider now the comparison of HCC[•]/HCCH to CNCH₂[•]/H₃CCN in entries 4 and 5. The BDE_{C-H} of acetylene is huge compared with the corresponding BDE_{C-H} of acetonitrile, and nevertheless, the identity barrier for the later reaction is significantly larger than the former. The reason is seen again to be the corresponding RE_X quantity. The acetylide radical behaves like a monoatomic radical; it is stiff and localized and hence its RE_{HCC} quantity is vanishingly small, 0.1 kcal/mol. By contrast, CNCH₂[•] is flat and delocalized and when it makes a bond it undergoes pyramidalization and electron localization; its RE_{CNCH_2} quantity is high, and this is the reason why the barrier for the CNCH₂[•]/H₃CCN is larger. In fact, radical chemists use acetonitrile as a solvent for HAT reactions because of the relative inertness of this solvent to HAT reactivity. Now we can see that what causes this functionality of acetonitrile is the large reorganization energy of the CNCH₂[•] radical.

Inspection of other reactions in Table 1 (entries 6, 10-12) reveals that the largest identity barriers are invariably found for those cases where the reorganization energy of the

radical is large. Clearly, the major factor of the identity barrier is RE_x , which is the preparation energy of the radical for bonding. Its effect comes about through the raising of the promotion energy of the reaction.

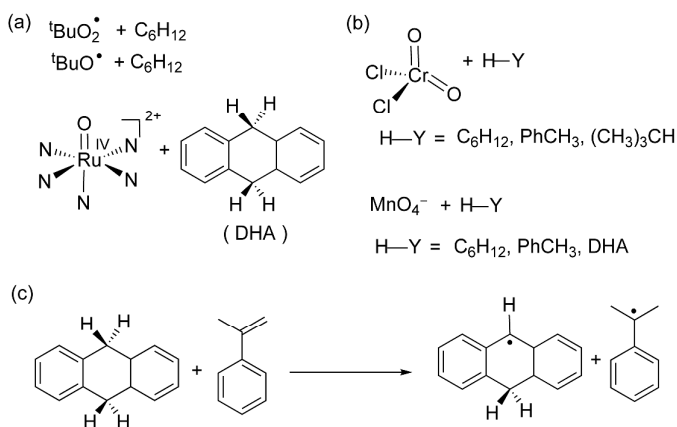
One interesting note regards the identity reaction $HO^*/H-OH$ (entry 8). It is seen that here the VB model predicts a significantly higher barrier than CCSD(T)/CBS. As we shall show later, this is associated with the blending of PCET character into the HAT TS. Furthermore, the CCSD(T)/CBS barrier is significantly higher than the experimental value, and as can be read from footnote [h] to the Table, the experimental barrier is sliced by tunneling.

4.2 Nonidentity HAT Reactions

Since the set of 45 reactions in Figure 11 involves plenty of nonidentity reactions, it appears that the VBSCD handles these reactions reasonably well. Furthermore, this means that equation 14 involves most likely the physically meaningful quantities that determine the barrier height.

In our recent review,¹⁷ we tried something still more ambitious, namely, predicting the barriers of experimental nonidentity reactions, which involve a set of open-shell abstractors and closed-shell ones, as shown in Scheme 2. Open-shell abstractors as in Scheme 2a seem to be natural H-abtractors, whereas closed-shell abstractors like dichlorochromium dioxide, α -methyl styrene, permanganate salts, etc. in Scheme 2b, seem less natural H-abtractors. Nevertheless, HAT reactivity with closed-shell abstractors has been noted in the early 1960s by Wiberg, and later by Ruchardt, Mayer, and Limberg, who used dichlorochromium dioxide, α -methylstyrene, permanganate salts, etc., and showed that these closed-shell molecules could participate in HAT with alkanes. The difference between open-shell and closed-shell abstractors has aroused much interest in recent years, and led to discussions about the role, if any, of the radical species of the abstractor.^{39,40} The corresponding data are placed in the ESI (see Figure S4, Tables S6

and S7), while for the sake of tutoring we focus on a particular comparison that will elucidate the problem (for more reading consult Refs. 17 and 28).



Scheme 2. HAT reactions: (a) For open-shell abstractors. (b,c) For closed-shell abstractors.

Let us compare two cases of HAT reactivity, one for open-shell and the other for closed-shell abstractors. To make the comparison meaningful, we require the two abstractors to possess *the same or nearly the same thermodynamic driving forces for HAT*. As may be seen from the ESI, CrO_2Cl_2 and ${}^t\text{BuOO}^{\bullet}$ have rather close *BDEs* (in fact, the DFT computed $BDE_{\text{CrO-H}}$ is slightly higher than $BDE_{\text{BuOO-H}}$) and hence these abstractors are ideal for our purpose. Figures 13a and 13b compare the H-abstraction reactions of CrO_2Cl_2 and ${}^t\text{BuOO}^{\bullet}$ towards the same alkane H-Y. Since CrO_2Cl_2 is a closed-shell molecule with two $\text{Cr}=\text{O}$ double bonds, the only way to eventually make the new O-H bond and create a Cr^{\bullet} radical is to decouple the $\text{Cr}=\text{O}$ bond into a triplet as shown in Figure 13a. Thus in the promoted state the triplet ${}^3\text{Cr}-\text{O}^{\bullet}$ and $\text{H}^{\bullet}-\text{Y}$ are paired such that the oxyl radical of $\text{Cr}-\text{O}^{\bullet}$ pairs the H^{\bullet} moiety to form a new bond pair and a singlet diradical (one electron on Cr^{\bullet} which has d^1 configuration and the other on Y^{\bullet}). By contrast, in Figure 13b, where the ${}^t\text{BuOO}^{\bullet}$ abstractor is already a radical, the promotion energy at the reactant side involves only the H-Y bond.

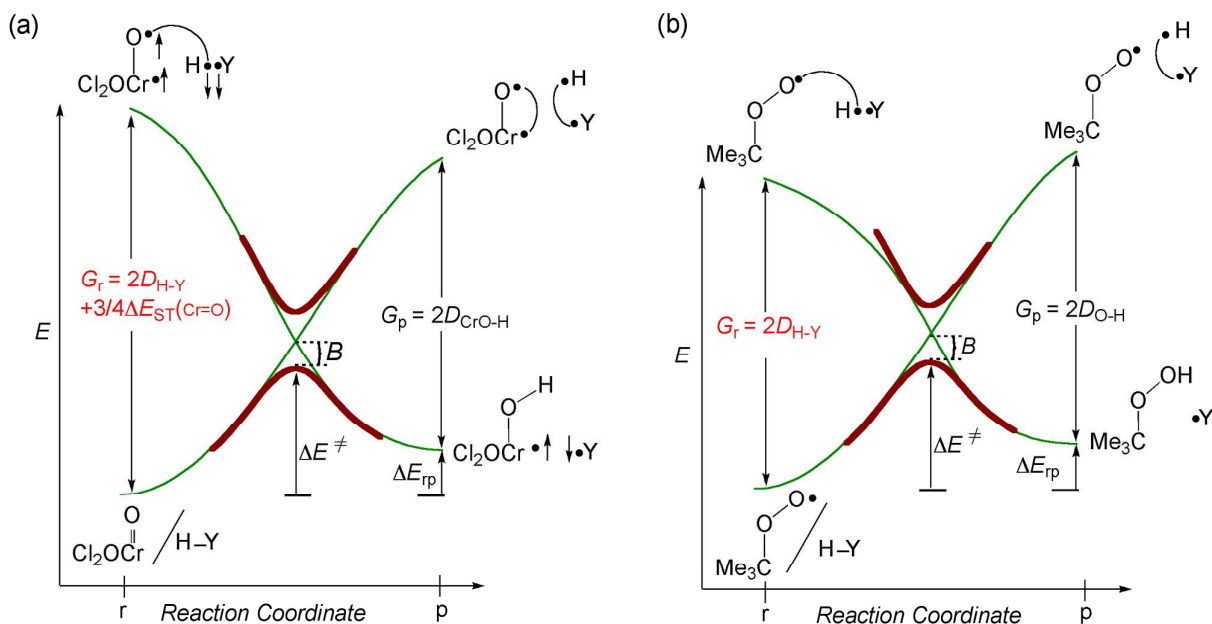


Figure 13. VBSCDs for HAT reactions of (a) the closed-shell CrO_2Cl_2 reagent, and (b) ${}^t\text{BuOO}^\bullet$, with an alkane H-Y . Not the additional promotion energy for the closed-shell reaction. Adapted with permission from Figure 4 in ref. 17.

It is very clear that with all other factors being identical, the barrier for the closed-shell abstractor will be raised in proportion to this additional promotion energy, proportional to $\Delta E_{\text{ST}}(\text{CrO}_2\text{Cl}_2)$. As such, the difference in the two barriers will derive solely from the value of the additional singlet-triplet excitation required to convert the closed-shell CrO_2Cl_2 into a ${}^{\bullet}\text{Cr-O}^\bullet$ diradical, namely:

$$\Delta E_{\text{VB}}^\ddagger(\text{CrO}_2\text{Cl}_2) - \Delta E_{\text{VB}}^\ddagger({}^t\text{BuOO}^\bullet) \approx (3/8)f_0\Delta E_{\text{ST}}(\text{CrO}_2\text{Cl}_2) \quad (17)$$

Using the experimental datum, $\Delta E_{\text{ST}}(\text{CrO}_2\text{Cl}_2) = 55.3$ kcal/mol, while DFT calculations lead to $\Delta E_{\text{ST}}(\text{CrO}_2\text{Cl}_2) = 40.1\text{--}45.0$ kcal/mol depending on the basis set used. Plugging the $\Delta E_{\text{ST}}(\text{CrO}_2\text{Cl}_2)$ values into equation 17, yields an energy barrier differences of $\Delta\Delta E_{\text{VB}}^\ddagger(\text{CrO}_2\text{Cl}_2 - {}^t\text{BuOO}^\bullet) = 4.5\text{--}6.2$ vs. a difference of experimental free energies of 7.4 kcal/mol.¹⁷

An important conclusion from the case in Figure 13 can be stated as Rule 3:

Rule 3: Even though the reverse reaction of a closed-shell abstractor involves an open-shell abstractor, the presence of a closed-shell abstractor for the forward reaction raises both the forward and reverse barriers to the same extent, as in Figure 13a. *It therefore fundamentally matters if the abstractor in a given reaction direction is closed-shell or both forward and reverse directions have only open-shell abstractors.*

In the general case, where all the barrier factors change between the closed-shell and open-shell abstractors, the difference in the corresponding barriers will reflect these various changes, which can be easily estimated with the following equation, which derives from eq. 14 (without the quadratic term) by adding additional promotion of the closed-shell abstractor, given in eq., 18 as $\Delta E_p(X)$:

$$\Delta E_{VB,XY}(1)^\ddagger = 0.3(D_{H-Y} + [\frac{1}{2}(\Delta E_p(X)) + D_{X-H}] + \frac{1}{2}(BDE_{H-Y} - BDE_{H-X}) - \frac{1}{4}[BDE_{H-X} + BDE_{Y-H}]);$$

$$\frac{1}{2}\Delta E_p(X) = 3/8[\Delta E_{ST}(X)] \quad (18a)$$

$$\Delta E_{VB,XY}(1)^\ddagger = 0.55BDE_{H-Y} - 0.45BDE_{H-X} + 0.3(RE_{X\cdot} + [\frac{1}{2}(\Delta E_p(X)) + RE_{Y\cdot}]) \quad (18b)$$

Collecting all the identical terms, we get equation 18b, which is analogous to equation 16 for identity reactions, showing that the barrier depends dominantly on the reorganization energy terms of the radicals $Y\cdot$ and $X\cdot$, and on the closed-shell abstractor ($\Delta E_p(X)$).

5. Some Generalities About Reactivity Patterns

At this point, it is appropriate to top this tutorial review with a few generalities. The first kind will deal with what we call in chemistry: *kinetic vs. thermodynamic control of chemical reactivity*, in which we'll outline the "kinetic" vs. "thermodynamic" factors in the VB model. In the second kind we shall present, albeit very briefly, *the effect of excited states on chemical reactivity* and demonstrate the blending of the several VB configurations (VBCMD) which shall help to understand the relationship between HAT and PCET dichotomy.^{17,28,32}

5.1. Thermodynamic vs. Kinetic Controls in Chemical Reactivity

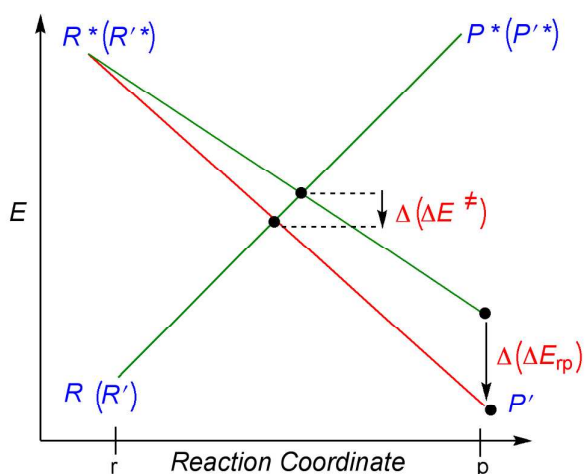
5.1.1 The Bell-Evans-Polanyi (BEP) and the Promotion Energy Gap (PEG)

Principles: The BEP principle^{17,27,40} states that the reaction will generally become faster as it is made more exothermic/exergonic. This is a statement of thermodynamic control. This principle has been widely used in radical additions to olefins and understandably met with mixed success.⁴¹⁻⁴³ However in HAT reactivity, the BEP principle has been usefully employed by experimentalists⁴⁰ to correlate the rate data of e.g. a single abstractor with a series of alkanes of varying BDE_{C-H} . Figure 14a shows the “pure” BEP principle, in an idealized case where a change from one product P to another P' stabilizes the product state relative to the reactant's, without affecting anything else. Hence, this change increases the thermodynamic driving force, i.e., the reaction becomes more exothermic (or exergonic), and lowers the crossing point. Assuming there is no other change, the lowering of the crossing point will lower also the barrier, ΔE^\ddagger , in proportion to the change in ΔE_{rp} , i.e. there is a “thermodynamic control” of the barrier. Since at the vicinity of the crossing point we can take the two curves as being linear,²⁰ we can write the following expression:

$$\Delta\Delta E^\ddagger/\Delta\Delta E_{rp} = \alpha = 1/2 \quad (19)$$

Thus, the “pure” idealized BEP principle predicts that the Brønsted parameter α in a reaction series, which purely obeys the BEP principle will be $1/2$, namely the barrier will change by one half of the change in the ΔE_{rp} . In fact, this is already clear from equation 9 for the barrier, namely, that the slope of such a ΔE^\ddagger vs. ΔE_{rp} plot should be $1/2$ assuming that all other factors in the equation are independent of ΔE_{rp} , precisely as we are doing here Figure 14a in the pictorial presentation of the BEP principle. But already now it is clear that this idealized situation is seldom met...

(a) The BEP Principle- Thermodynamic Control



(b) The PEG Principle- Kinetic Control

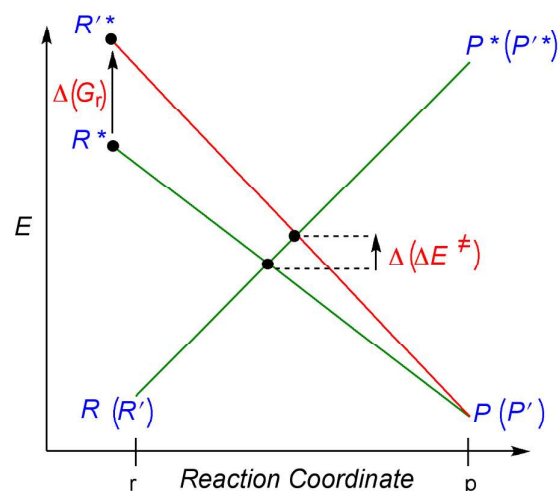


Figure 14. Simplified VBSCD's using straight lines and omitting the avoided crossing. The unprimed and primed symbols represent e.g., R changing to R' and P to P' , etc. (a) A plot of the “pure” BEP Principle, where the only change is the stabilization of the product state P to P' , which exerts thermodynamic control of reactivity. (b) A plot of the “pure” PEG Principle, where the only change is the raising of the promoted state on the reactant side from R^* to R'^* , which exerts kinetic control of reactivity.

The foregoing discussion considers only the relative energies of R and P , while a kosher treatment must consider the four states in the VBSCD in an equivalent manner. Primarily, the promotion energy gaps (PEG) are the root causes why we have a barrier at all, and hence one must consider the PEG effects due to a change in the nature of the reactants. The “pure” PEG principle is related to the change of the barrier due to a change in one of the promotion gap or in both, and is a statement of “kinetic control” of reactivity. Figure 14b illustrates the “pure” PEG principle by considering the effect of the increase of G_r . It is seen that this will raise the crossing point, and in the case where no other effect coexists, this will raise the barrier (and vice versa when G_r decreases). Thus, in complete analogy with the Brønsted parameter for thermodynamic effect on reactivity, we can define a *promoted-state parameter* α^* that gauges the slope of the kinetic control effect in a reaction series. For the case in Figure 14b, it is given by equation 20, and in the linear approximation of the VB states near the crossing point, it would be equal to $\frac{1}{2}$ (but for general curves it will depend on f_0 , see eq. 9):

$$\alpha^* = \Delta\Delta E^\ddagger / \Delta(G_r) \approx \frac{1}{2} \quad (20)$$

In Figure 13 above, we treated such an example, where the promotion gap, G_r , was increased by the reorganization energy of the closed-shell abstractor CrO_2Cl_2 . It is seen from Figure 14b that the increase of G_r will raise the barriers in both the forward and reverse directions. Of course, lowering the promotion gaps will lower these barriers. We can call these effects due to changes in the promotion energy gap as the “**PEG Principle**”.

5.1.2 Entangled Effects: From the applications of the model to HAT reactivity, it is very clear that if we accept the barrier equation (eq. 14) to be physically meaningful, we must then admit that the *BDE* quantities appear in the promotion energies as well as in the thermodynamic driving force of the reaction and in the *B* factor. As such, the factors that govern the HAT barriers are not independent of each other. And hence, the BEP and PEG effects in a given experimental reaction series are completely entangled. Since the BEP principle is widely used in the HAT community, because of the facility of determining *BDEs* using the Bordwell equation, it is essential to look more closely at the consequences of this entanglement.

This change in ΔE_{rp} for HAT essentially reflects the fact that the *BDEs* of the reactant or of product change; either the *BDE* for the forming bond H-X becomes larger, or the *BDE* for the bond in the reactant, H-Y, gets smaller. However, as the *BDE* determines also the promotion gap (eqs. 10 and 14), any change in ΔE_{rp} due to a change in *BDE* will be attended by changes in G_r and G_p . This is shown in Figure 15, for a case where the bond H-Y becomes weaker, and leads to increase of the thermodynamic driving force, while decreasing the promotion gap at the reactant side by double this amount (see G_r expression in eqs. 3 and 10).

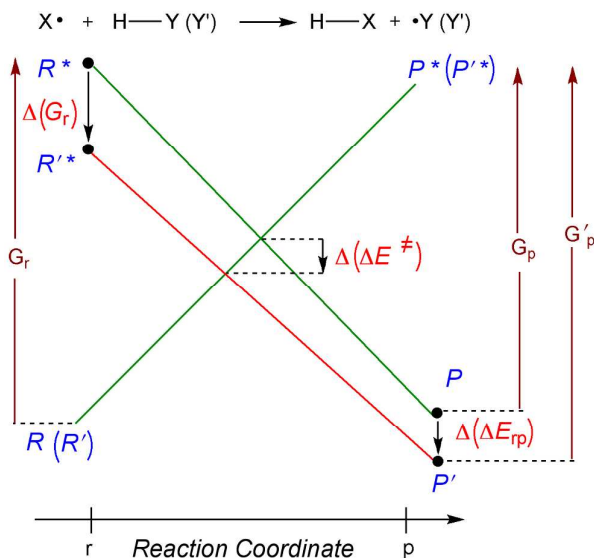


Figure 15. Entangled reactivity: the change in ΔE_{rp} due to replacement of Y by Y' (P to P') is expressed twice as much in G_r [$\Delta(G_r) = 2(\Delta\Delta E_{rp})$]. Assuming no other factor changes, the plot of ΔE^\ddagger vs. ΔE_{rp} will yield an entangled slope.

If we neglect the quadratic term and disregard any change in B , we can see that in this case, a BEP plot (of ΔE^\ddagger vs. ΔE_{rp}) will have a slope that starts being larger than unity (assuming linear lines) for low G_r values, and converges to 0.75 when G_r is much larger than $\Delta\Delta E_{rp}$:

$$\Delta\Delta E^\ddagger/\Delta\Delta E_{rp} = \frac{1}{2} \Delta\Delta E^\ddagger/\Delta(G_r) = \alpha \alpha^* > 1 \quad (21a)$$

$$\Delta\Delta E^\ddagger/\Delta\Delta E_{rp} = \frac{1}{2} \Delta\Delta E^\ddagger/\Delta(G_r) = \alpha \alpha^* \rightarrow 0.75 \quad (G_r \gg |\Delta\Delta E_{rp}|) \quad (21b)$$

Using other curve types yields values that even mascaared the pure BEP effect, $\alpha \alpha^* \sim 0.5$, despite of the fact this is not a pure BEP case. For sure this is not a Brønsted parameter due to a BEP effect. It is primarily a PEG effect. Since many of the experimental reaction series are based on changes in $BDEs$, this entangled BEP/PEG effect will be very common in HAT reactions, and will reflect in fact a dominant PEG effect.

One can think of other variations in the promotion gaps and derive the expected slopes for the respective “BEP plots”. These slopes will not reflect true BEP effects, but rather PEG effects or entangled effects, which are not easy to resolve. This of course does

not mean that the BEP principle is useless as a practical guide for designing viable HAT experiments. *It only means that it is not fundamental and it cannot be resolved from the primary PEG principle.*

5.2. VBCMD and Excited-State Effects on Reactivity Patterns

The emphasis on the BEP principle in HAT is a seductive simplicity. Nevertheless, if we resist this temptation we'll recognize that there is a general and important effect of excited states on reactivity. This effect does not stop at the promoted states effect. In fact, we alluded already to the mixing of excited states into the principal curves in the VBCMD (Figures 1b,c). Here we simply want to generalize this important effect by mentioning a few examples.

Let us start with the beautiful example of Woodward-Hoffmann forbidden and allowed cyclization of butadiene to cyclobutene. The reaction can transpire in two stereochemical manners; one is the allowed con-rotatory (CON) cyclization, the other is the forbidden dis-rotatory (DIS) cyclization. The CON pathway is preferred over the DIS pathway by ~20 kcal/mol or so. As shown in Figure 16, this is a case where the thermodynamic driving force is the same for the two pathways and the promotion gaps are identical.²⁹ What makes the difference is a CT state that can mix into the CON TS, but its mixing into the DIS TS is symmetry forbidden.

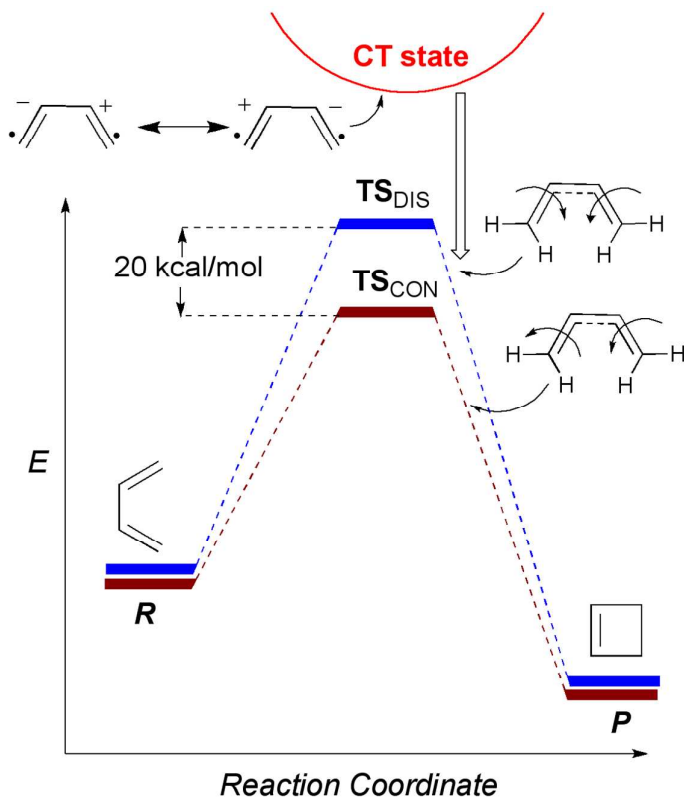


Figure 16. The conrotatory (CON) and disrotatory (DIS) pathways of butadiene cyclization. The TS for the CON pathway is lower in energy due to symmetry allowed mixing with the higher lying charge transfer (CT) state.¹⁴ The CT state is shown schematically as involving electron transfer from one double bond to the other.

The impact of CT state mixing was demonstrated above in the examples of aromatic and olefin activations by Cpd I of P450 (Figure 9 and S1), where a low-lying CT state affected the resonance energy of the TS and the barrier of the reaction. The CT effect was also briefly mentioned in the HAT reactions by P450, where the best electron donor substrates (**8** and **14**, Figure 5) deviated from eq. 7. In fact, CT effects are expected in any other reaction where the principal VB state curves do not involve redox (see definition in **Textbox 1**), e.g., in radical addition to olefins.⁴² This can be stated in Rule 4:

Rule 4: All of the reactions wherein the promoted states are “covalent” in character (no redox, see **Textbox 1**) possess intermediate-state curves made from CT states. These CT states can potentially affect reactivity, depending on the donor-acceptor relationship of the reactants.

5.3. Excited State Effects on HAT reactivity-The Proton-Coupled Electron Transfer (PCET) Mechanism

In accord with **Rule 4**, HAT reactions possess CT excited states, which correspond to electron transfer/proton transfer state curves.^{14,16,17} Generally, the CT states are high in energy and have little effect on reactivity, but occasionally they become very important and descend below the covalent HAT curves and thereby lead to the concerted PCET mechanism.^{17,28,32,44} Let us first understand the HAT/PCET dichotomy, and then proceed to construct the corresponding VB diagrams.

Figure 17 shows the difference between a normal HAT and PCET for a pair of alkoxy radicals exchanging an H atom. Figure 17a, shows the normal HAT, by decoupling the electrons of the O-H bond and recoupling them with the oxyl center. This leads to 3-center/3-electron TS, where the unpaired electron resides in a nonbonding orbital ϕ_{σ}^{-} that involves a node on the H in transit. However, as shown in Figure 17b, since the oxyl center has also free lone pairs, it can utilize one of the lone pairs to abstract a proton from the O-H bond, such that it forms a three-center/4-electron O---H---O σ -species, while the unpaired electron undergoes delocalization in the ϕ_{π}^{-} orbital. Thus, in Figure 17b we have a proton-coupled electron transfer, where the proton is exchanged along the σ -axis and the electron is transferred via the π orbitals.^{17,28,32,45}

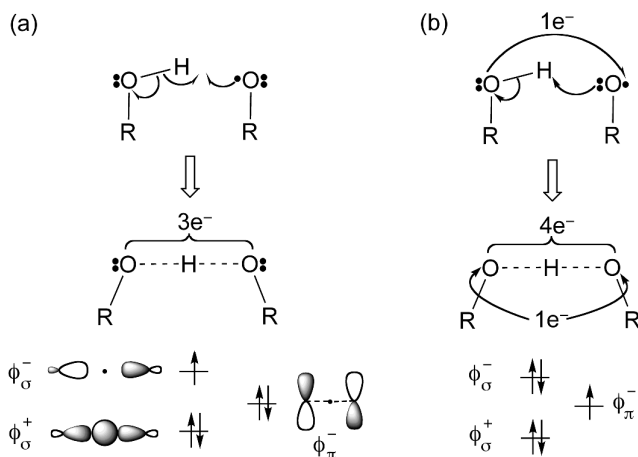


Figure 17. H exchange between two alkoxy radicals, by; (a) normal HAT, and (b) PCET. In each case we show the highest-lying orbitals and their occupancy in the respective TSs. Adapted with permission from Scheme 3 in ref.17.

The VB diagrams describing the HAT/PCET dichotomy are depicted in Figure 18, which shows three cases of H-atom exchange between radicals with intermediate-state curves as specified in Rule 4. These diagrams are VBCMDs that display two sets of intersection curves; one set in the full lines involves the normal HAT curves, where the promoted states are labeled as $\Psi_{\text{HAT},r}^*$ and $\Psi_{\text{HAT},p}^*$, while the other set in the dotted lines is denoted as $\Psi_{\text{CT},r}^*$ and $\Psi_{\text{CT},p}^*$ (the corresponding $n\sigma^*$ states will also interfere, but are kept out of the Figure to keep it relatively simple) This latter set of curves corresponds to proton transfer (PT) between the radicals and have a mixed PT/ET nature.

Figure 18a, describes the situation for two methoxyl radicals exchanging H. We can see that the reactants and products of the dotted curves are PT species, and the corresponding promoted states are CT states wherein the corresponding MeO^\bullet radical transfers an electron, from one of its lone pairs, to the O-H bond in methanol.^{17,29} The lower pair of state curves describes the normal HAT curves. Since the two pairs of curves are not too far in energy, the PCET curves mix into the HAT TS, lower it in energy and endow it with some PT character.

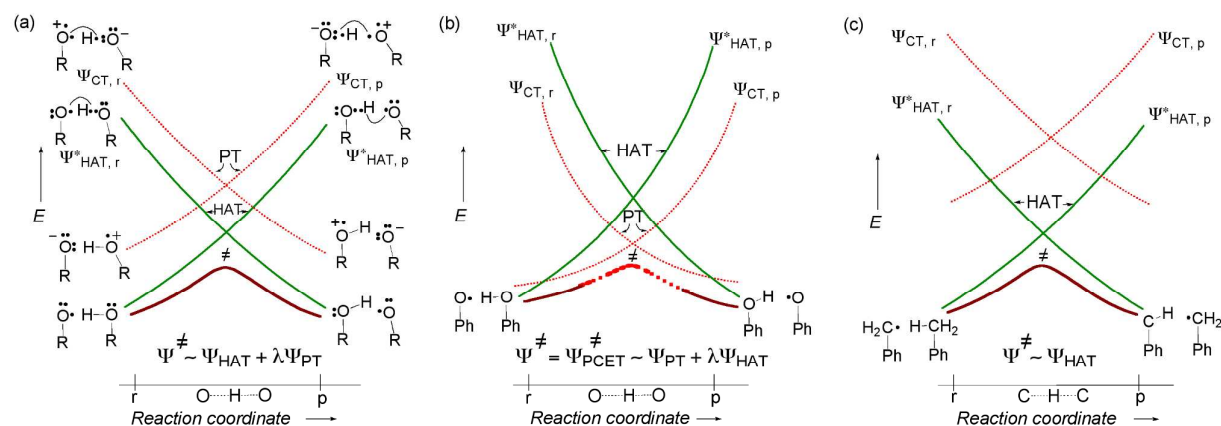


Figure 18. VBCMDs describing the hybrid HAT/PCET dichotomy to mixing of normal HAT VB states (in green), and proton transfer (PT) curves (in red dotted lines), along the reaction coordinate. For simplicity we show on the oxygen *only the one lone pair* that participates in the PCET. The PT/ET curves are anchored in charge transfer (CT) promoted states of reactants and products, indicated as $\Psi_{\text{CT},r}$ and $\Psi_{\text{CT},p}$, and their lower points are PT species. (a) A case of two methoxyl radicals exchanging H. Here the CT states lie higher than

the HAT states, $\Psi_{\text{HAT},r}$ and $\Psi_{\text{HAT},p}$. Assuming no symmetry restrictions, the wave function of the TS (Ψ^\ddagger) has a dominant HAT character with a secondary PT character. (b) A case where two phenoxyl radicals exchange H. Here, the CT curves are low-lying and descend below the crossing point of the HAT curves. The corresponding TS is now a PCET-type with a predominant PT character and a secondary HAT character. The mixing of the two state-sets transforms smoothly from a PT to a HAT state, at the two diagram ends. (c) A case of two benzyl radicals exchanging H. Here the PT/ET curves are high lying and do not mix effectively into the HAT TS.

Figure 18b shows the situation for two phenoxyl radicals exchanging H. Here the ET/PT curves are low in energy, and they cross the HAT curves below the crossing point of the latter curves. The mixing of the four curves creates a PCET TS, with a dominant PT character and a small HAT character. Note that near the reactants and products, the HAT curves cross below the PT/ET curves, thus generating an energy profile, which changes characters from PCET at the TS to HAT en route to either reactants or products.

The mechanistic choice in the two reactions in Figures 18a and 18b depends on the strength of the O-H bond, and the ionization potential (*IP*) of the lone pair in the RO^\bullet radical.^{17,28} A strong O-H bond will be a poor electron acceptor,^{14,29} and when the radical has a high $IP_{\text{RO}\cdot}$, the two effects together generate high-lying CT states, and vice versa when the O-H bond is weak and the $IP_{\text{RO}\cdot}$ is low. The O-H bonds of alkyl alcohols are ~ 20 kcal/mol stronger than O-H bonds of phenols, and the corresponding *IP* value for alkoxy lone-pair is higher than for phenoxyl, and as such the $\text{PhO}^\bullet/\text{PhO-H}$ pair proceeds via PCET (as in Figure 18b) while the $\text{CH}_3\text{O}^\bullet/\text{CH}_3\text{O-H}$ pair undergoes HAT (as in Figure 18a) with some PCET character blended into the TS. Clearly, one may expect a spectrum of cases that differ in the amounts of PCET and HAT character and depend on the chemical identity of the radical and the H-donor molecule.

An interesting feature of the HAT/PCET blending is the finding that generally phenoxyl radicals abstract H or exchange H much faster than corresponding alkyl radicals.^{17,28,32,40} The reason becomes apparent from Figure 18c, which describes the H-exchange in $\text{PhCH}_2^\bullet/\text{PhCH}_3$. Here it is apparent that the ET/PT curves are too high lying to mix effectively into the HAT TS, because the C-H bond is generally a poor electron acceptor, and because the radical does not have an electron pair with a sufficiently low *IP* to support sufficiently low CT state curves. As such, the reaction of $\text{PhCH}_2^\bullet/\text{PhCH}_3$ does

not enjoy the added stabilization due to the PCET/HAT blending and its barrier is significantly higher than that for the PhO[•]/PhO-H pair.

We recently showed how iron^{IV}-oxo reagents that are typified by substantial basicity prefer invariably the PCET mechanism.³² One sign of this preference is the BEP plot which is generally linear for normal HAT reactions becomes completely scattered. Such a plot is shown in Figure 19. Inspection of the Figure further reveals that the H-abstraction barriers for C-H bonds (in substrates, **S1**, **S2**, **S5**) are higher than those for N-H and O-H bonds, at the same thermodynamic driving force (e.g., compare **1+S1** to **1+S3** and **S4**). These lower barriers for N-H and O-H bonds reflect the mixing of the ET/PT with HAT states at the TS region.

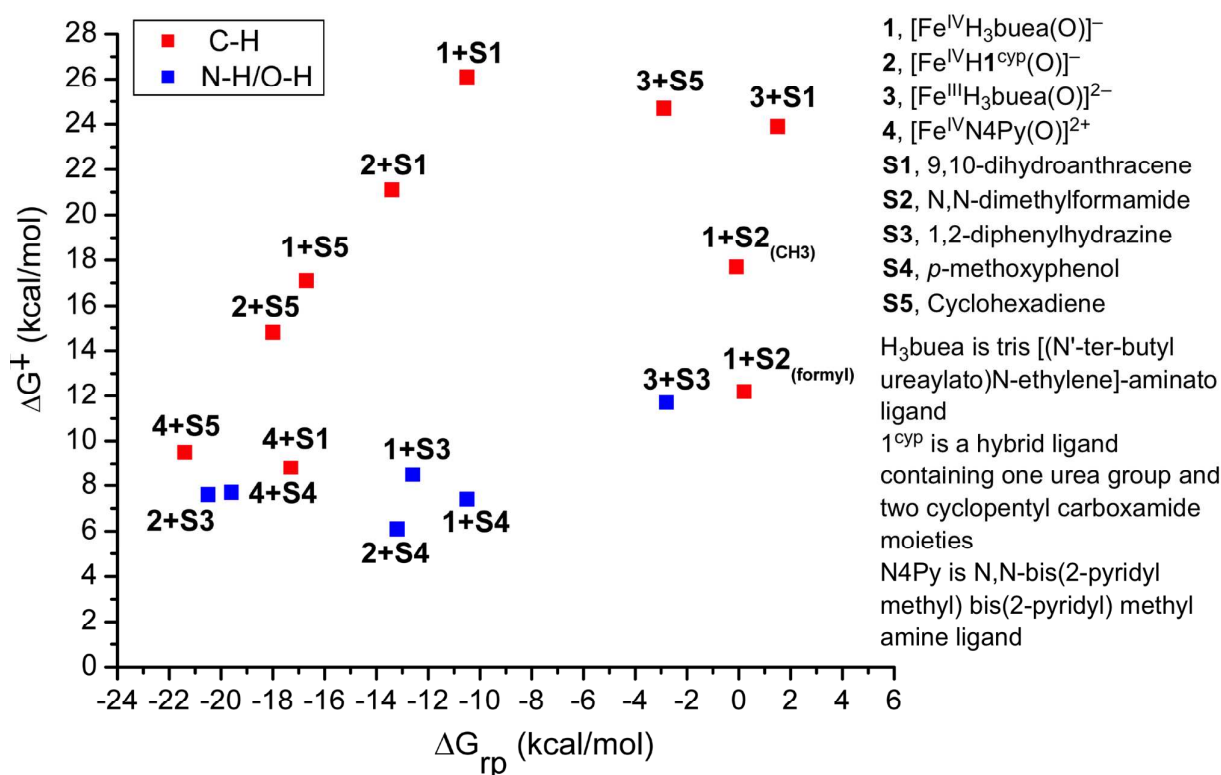


Figure 19. (a) A scattered BEP plot for H-abstraction by four iron-oxo reagents having variable basicity; $4 < 2 < 1 < 3$, reacting with C-H (**S1**, **S2**, **S5**), N-H (**S3**) and O-H bonds (**S4**). Adapted with permission from Figure 4 in ref. 32.

Clearly, the VBCMD models in Figure 18 provide an attractive unification for the HAT/PCET reactivity spectrum. The notion of blended HAT/PCET reactivity, which

emerges from the VB model, has many interesting consequences, which are discussed in the original literature.^{17,28,32}

6. Concluding Remarks

The valence bond approach to chemical reactivity accounts for the reorganization of the electrons and bonds along the potential energy profile. As such, it provides the qualitative physics of the transition state as an “egg state” that arises due to the mixing of the reactants-, products- and excited-states, and that can as such evolve to reactants and products along the energy profile. Because of this feature, the model allows you to estimate barriers quantitatively from the raw data, predict mechanisms, and unify rich reactivity patterns. It enables to see the forest from the trees.

Valence bond modeling is thus a useful interface between experiment and theory, and between computations (generating numbers) and understanding them. It makes a connection between quantum mechanics and the experimental notions of thermodynamic vs. kinetic controls of reactivity. It creates bridges to physical organic chemistry concepts like the BEP principle, and orbital symmetry conservation, while at the same time revealing new principles such as the PEG principle and the essential role of excited state in ground state reactivity. The treatment of photochemical reactivity,^{14,29} which naturally emerges from the VBSCD and VBCMD models, is left for a future tutorial.

We tried to project all these attractive features by focusing on the H atom transfer reaction and highlighting its rich reactivity landscape where excited states seem to have substantial influence on the reactivity and mechanism. Having done all that, we can only hope that the tutorial will be deemed useful to the teachers and students of the chemical community, even if it does not obviously describe the entire richness of VB theory⁴⁶⁻⁵⁰ and its application to chemical reactivity.

Acknowledgements SS thanks Zenhua Chen and Mark Danovich for their help with quantitative aspects of intersecting curves. The HU research is supported by the ISF (grant 53/09).

References

1. F. Hund, *Z. Phys.*, 1931, **73**, 1; F. Hund, *Z. Phys.*, 1928, **51**, 759.
2. J. H. van Vleck, *J. Chem. Phys.*, 1935, **3**, 807.
3. L. Pauling, *The Nature of the Chemical Bond*, Cornell University Press, Ithaca, New York, 1939 (3rd ed., 1960).
4. K. Fukui, T. Yonezawa and H. Shingu, *J. Chem. Phys.*, 1952, **20**, 722.
5. R. B. Woodward and R. Hoffmann, *The Conservation of Orbital Symmetry*, Verlag Chemie, Weinheim, 1971.
6. H. Chen, D. Danovich and S. Shaik in *Comprehensive Inorganic Chemistry II*, ed. J. Reedijk and K. Poeppelmeier, Elsevier, 2nd edn., 2013, vol. 9, ch.1, pp 2.
7. S. Shaik, *New. J. Chem.*, 2007, **31**, 2015.
8. S. Shaik, *J. Am. Chem. Soc.*, 1981, **103**, 3692.
9. S. Shaik and A. Pross, *J. Am. Chem. Soc.*, 1982, **104**, 2708.
10. A. Pross and S. Shaik, *Acc. Chem. Res.*, 1983, **16**, 363.
11. S. S. Shaik, *Prog. Phys. Org. Chem.*, 1985, **15**, 197.
12. S. Shaik, H. B. Schlegel and S. Wolfe, *Theoretical Aspects of Physical Organic Chemistry. Application to the S_N2 Transition State*, Wiley Interscience, NY, 1992.
13. S. Shaik and P. C. Hiberty, *Adv. Quant. Chem.*, 1995, **26**, 99.
14. S. Shaik and A. Shurki, *Angew. Chem. Int. Ed.*, 1999, **38**, 586.
15. S. Shaik, *Phys. Chem. Chem. Phys.*, 2010, **12**, 8706.
16. S. Shaik, W. Z. Lai, H. Chen, Y. Wang, *Acc. Chem. Res.*, 2010, **43**, 1154.
17. W. Z. Lai, C. Li, H. Chen, S. Shaik, *Angew. Chem. Int. Ed.*, 2012, **51**, 5556.

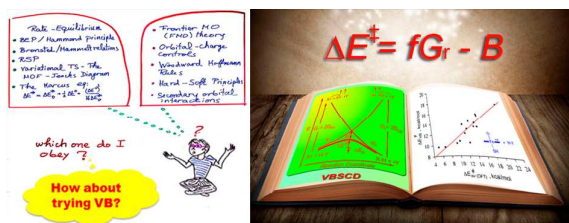
18. G. Sini, S.S. Shaik, J.M. Lefour, G. Ohanessian and P.C. Hiberty, *J. Phys. Chem.*, 1989, **93**, 5661.
19. S. Shaik, W. Wu, K. Dong, L. Song and P. C. Hiberty, *J. Phys. Chem. A*, 2001, **105**, 8226.
20. L. Song, W. Wu, K. Dong, P.C. Hiberty and S. Shaik, *J. Phys. Chem. A*, 2002, **106**, 11361.
21. L. Song, W. Wu, P. C. Hiberty, D. Danovich and S. Shaik, *Chem.–Eur. J.*, 2003, **9**, 4540.
22. L. Song, W. Wu, P. C. Hiberty and S. Shaik, *Chem.–Eur. J.*, 2006, **12**, 7458.
23. P. Su, L. Song, W. Wu, P. C. Hiberty and S. Shaik, *J. Am. Chem. Soc.*, 2004, **126**, 13539.
24. W. Wu, P. Su, S. Shaik and P. C. Hiberty, *Chem. Rev.*, 2011, **111**, 7557.
25. S. Shaik, D. Kumar and S. P. de Visser, *J. Am. Chem. Soc.*, 2008, **130**, 10128
Correction: 2008, **130**, 14016.
26. S. Shaik, Y. Wang, H. Chen, J. Song and R. Meir, *Faraday Discuss.*, 2010, **145**, 49.
27. P. Milko, P. Schyman, D. Usharani, H. Chen and S. Shaik, *J. Chem. Theory Comput.*, 2011, **7**, 327.
28. C. Li, D. Danovich and S. Shaik, *Chem. Sci.*, 2012, **3**, 1903.
29. S. Shaik and P. C. Hiberty, *A Chemist's Guide to Valence Bond Theory*, John Wiley & Sons Inc., New York, 2008.
30. S. Shaik, S. Cohen, Y. Wang, H. Chen, D. Kumar, and W. Thiel, *Chem. Rev.*, 2010, **110**, 949.
31. H. B. Dunford, *Heme Peroxidases*, Wiley-VCH, New York, 1999.
32. D. Usharani, D. C. Lacy, A. S. Borovik and S. Shaik, *J. Am. Chem. Soc.*, 2013, **135**, 17090.
33. D. Kumar, B. Karamzadeh, G. N. Sastry and S. P. de Visser, *J. Am. Chem. Soc.*, 2010, **132**, 7656.

34. K. Yamaguchi, Y. Takahara and T. Fueno, in *Applied Quantum Chemistry* ed. V. H. Smith, Jr., H. F. Schaefer III and K. Morokuma, Reidel, Dordrecht, 1986, pp 155.
35. E. A. Carter, W. A. Goddard III, *J. Phys. Chem.*, 1988, **92**, 2109.
36. S. Shaik, M. Filatov, D. Schröder and H. Schwarz, *Chem.–Eur. J.*, 1998, **4**, 193.
37. C. Li and S. Shaik, *RSC Adv.*, 2013, **3**, 2995.
38. C. M. Bathelt, L. Ridder, A. J. Mulholland and J. N. Harvey, *Org. Biomol. Chem.*, 2004, **2**, 2998.
39. N. Dietl, M. Schlangen and H. Schwarz, *Angew. Chem. Int. Ed.*, 2012, **51**, 5544.
40. C. T. Saouma and J. M. Mayer, *Chem. Sci.*, 2014, **5**, 21.
41. M. L. Poutsma, *J. Phys. Org. Chem.*, 2008, **21**, 758.
42. H. Fischer and L. Radom, *Angew. Chem. Int. Ed.*, 2001, **40**, 1340.
43. M. W. Wong, A. Pross and L. Radom, *J. Am. Chem. Soc.*, 1994, **116**, 6284.
44. A. Cembran, M.R. Provorse, C. Wang, W. Wu, J. Gao, *J. Chem. Theory. Comput.* **2012**, **8**, 4347–4358.
45. J. M. Mayer, D. A. Hrovat, J. L. Thomas and W. T. Borden, *J. Am. Chem. Soc.* 2002, **124**, 11142.
46. D. L. Copper, P. B. Kardakov and T. Thorsteinsson. *Modern Valence-Bond Description of Gas Phase Pericyclic Reactions*, in Valence Bond Theory, D. L. Cooper, Ed., Elsevier, Amsterdam, 2002, pp. 41-51.
47. M. A. Robb, M. Olivucci and M. A. Robb. *Adiabatic and Diabatic Surfaces in the Treatment of Chemical Reactivity. I. Theory*, in New Theoretical Concepts for Understanding Organic Reactions, J. Bertran and I. G. Csizmadia, Eds. NATO ASI Series, Kluwer Publ., Dordrecht, 1989, Series C267, pp. 101-146.
48. M. A. Robb, M. Garavelli, M. Olivucci and F. Bernardi. *A Computational Strategy for Organic Photochemistry*, in *Reviews in Computational Chemistry*, 2000, **25**, 87-46.
49. F. Faglioni and W. A. Goddard, III, *Intern. J. Quant. Chem.* 1999, **73**, 1.

50. J. P. Malrieu, R. Caballol, C. J. Calzado, C. de Graf and N. Guihéry, *Chem. Rev.*

2014, **114**, 429.

TOC: This tutorial teaches the interested how to comprehend and predict reactivity patterns in a variety of reaction types.



Biographical Sketchs



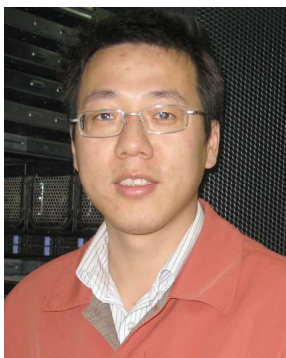
Dandamudi Usharani an Indian citizen by birth, won gold medal in chemistry in her B. Sc (1996), and obtained M. Sc in chemistry (1998) from University of Hyderabad. After a few years of college teaching (1998-2003) she joined the research group of Prof. E.D. Jemmis and obtained Ph.D (2009) in computational chemistry from the University of Hyderabad. She is currently working as a postdoctoral fellow with Prof. S. Shaik in the Hebrew University. Her main research interests are in electronic structure, bonding, and reactivity of organic, organometallic/bioinorganic complexes, and metalloenzymes with focus on fundamental and translational aspects to human health.



Wenzhen Lai received her B.Sc. (2002) in chemistry from Sichuan University, China. She obtained her M.Sc. (2005) in physical chemistry from Sichuan University and Ph.D. (2008) in theoretical and computational chemistry from Nanjing University under supervision of Prof. Daiqian Xie. After her postdoctoral studies at the Hebrew University of Jerusalem with Prof. Sason Shaik, she joined the Department of Chemistry, Renmin University of China as an associate professor in 2001. Her main research interests are focused on the reaction mechanisms of inorganic, biological and biomimetic systems.



Chunsen Li received his B.Sc. in chemistry (2001), M.Sc. (2004), and Ph.D. (2007) in physical chemistry from Xiamen University, China, with Prof. Wei Wu. Subsequently he joined the group of Prof. Walter Thiel at the Max-Planck-Institut für Kohlenforschung in Mülheim, Germany, as a postdoctoral fellow. In 2010 he moved to The Hebrew University of Jerusalem to work with Prof. Sason Shaik as a postdoctoral fellow. In the middle of October 2013, he joined the Fujian Institute of Research on the Structure of Matter (FJIRSM), in the Chinese Academy of Sciences, as a professor. His main research interests are in QM and QM/MM studies of metalloenzymes and functional materials.



Hui Chen received his Ph.D. (2006) from Nanjing University with Prof. Shuhua Li. He then worked with Prof. Sason Shaik as a postdoctoral fellow at the Hebrew University, where he won the Lise Meitner Prize of the Lise-Meitner-Minerva Center (2007) for computational quantum chemistry. In 2011, he joined Institute of Chemistry, Chinese Academy of Sciences (ICCAS) as a professor of chemistry where he leads a research group in ICCAS. His current main research interests include high level ab initio calculations, intriguing reaction mechanisms and complex electronic structures of both ground and excited states in chemistry and biochemistry, especially those involving transition metals.



David Danovich was born in Russia in 1959. He graduated in physics from Irkutsk State University in Russia in 1982 and obtained his Ph.D. degree in Quantum Chemistry therein 1989 under the guidance of Dr. Vyacheslav G. Zakrzewski and Prof. Vladimir K. Voronov. He was a postdoctoral fellow with Prof. Yitzhak Apeloig at Technion, Haifa, Israel, from 1990 to 1992. In 1992 he joined the group of Prof. Sason Shaik at the Hebrew University, where he is currently a senior computational chemist at the Lise Meitner Minerva Center for Computational Quantum Chemistry. His current research interests include theoretical studies of unusual chemical bonding based on the Valence Bond and high level *ab initio* approaches.

